NeuroImage 200 (2019) 674–689

Contents lists available at ScienceDirect

NeuroImage

journal homepage: www.elsevier.com/locate/neuroimage

Combining white matter diffusion and geometry for tract-specific alignment and variability analysis

Itay Benou [a,c], Ronel Veksler [b,c], Alon Friedman [b,c,d], Tammy Riklin Raviv [a,c,*]

[a] Department of Electrical and Computer Engineering, Ben-Gurion University of the Negev, Beer-Sheva, Israel
[b] Department of Physiology and Cell Biology, Ben-Gurion University of the Negev, Beer-Sheva, Israel
[c] The Zlotowski Center for Neuroscience, Ben-Gurion University of the Negev, Beer-Sheva, Israel
[d] Departments of Medical Neuroscience and Brain Repair Centre, Dalhousie University, Faculty of Medicine, Halifax, Canada

ARTICLE INFO

Keywords:
Diffusion MRI
White matter
Fiber bundle
Tract-specific analysis
Tractography registration
Mild traumatic brain injury

ABSTRACT

We present a framework for along-tract analysis of white matter (WM) fiber bundles based on diffusion tensor imaging (DTI) and tractography. We introduce the novel concept of fiber-flux density for modeling fiber tracts' geometry, and combine it with diffusion-based measures to define vector descriptors called Fiber-Flux Diffusion Density (FFDD). The proposed model captures informative features of WM tracts at both the microscopic (diffusion-related) and macroscopic (geometry-related) scales, thus enabling improved sensitivity to subtle structural abnormalities that are not reflected by either diffusion or geometrical properties alone. A key step in this framework is the construction of an FFDD dissimilarity measure for sub-voxel alignment of fiber bundles, based on the fast marching method (FMM). The obtained aligned WM tracts enable meaningful inter-subject comparisons and group-wise statistical analysis. Moreover, we show that the FMM alignment can be generalized in a straight forward manner to a single-shot co-alignment of multiple fiber bundles. The proposed alignment technique is shown to outperform a well-established, commonly used DTI registration algorithm. We demonstrate the FFDD framework on the Human Connectome Project (HCP) diffusion MRI dataset, as well as on two different datasets of contact sports players. We test our method using longitudinal scans of a basketball player diagnosed with a traumatic brain injury, showing compatibility with structural MRI findings. We further perform a group study comparing mid- and post-season scans of 13 active football players exposed to repetitive head trauma, to 17 non-player control (NPC) subjects. Results reveal statistically significant FFDD differences (p-values$<$0.05) between the groups, as well as increased abnormalities over time at spatially-consistent locations within several major fiber tracts of football players.

1. Introduction

Diffusion tensor imaging (DTI) and tractography are efficient tools for the study of white matter (WM), in particular when standard magnetic resonance imaging (MRI) is not sufficiently sensitive to detect subtle structural anomalies, such as in mild traumatic brain injury (mTBI) (Shenton et al., 2012). Fiber bundles rendered by tractography algorithms, in the form of 3D streamlines, can be represented by their geometrical features as well as diffusion-related measures (e.g., fractional anisotropy - FA, mean diffusivity - MD, axial diffusivity - AD, radial diffusivity - RD). Diffusion parameters have been shown to reflect local variations in WM properties at the *microscopic* scale (e.g., damage to myelin and axon membranes) (Basser and Pierpaoli, 2011), and were suggested to be effective measures in assessment of mTBI (Borja et al., 2018; Gorodissky et al., 2018). On the other hand, studies of head impact mechanism associated with TBI also show implications on WM structures at the *macroscopic* scale, i.e., affecting their shape, thickness, fiber density, and other physical measures (Bigler, 2018; Sharp et al., 2014). Evidence of such macrostructural variations in fiber bundles were demonstrated in DTI and tractography studies of TBI patients (Baugh et al., 2012; Håberg et al., 2015), as well as in subjects with other neurological disorders such as Amyotrophic Lateral Sclerosis (ALS) (Zhang et al., 2010). Therefore, while most WM variability studies focus on diffusion-based analysis, some recent techniques suggest incorporating macroscopic morphological analysis alongside microscopic features to achieve a more full-scale assessment of WM integrity (Zhang et al., 2010; Raffelt et al., 2017).

Using either microscopic or macroscopic properties, coherent

* Corresponding author. Department of Electrical and Computer Engineering, Ben-Gurion University of the Negev, Beer-Sheva, Israel.
E-mail address: tammy@csail.mit.edu (T.R. Raviv).

https://doi.org/10.1016/j.neuroimage.2019.05.003
Received 12 June 2018; Received in revised form 22 April 2019; Accepted 2 May 2019
Available online 13 May 2019

mathematical modeling of fiber bundles for quantitative inter-subject comparison and group-wise analysis, is a challenging task. The main difficulty is finding a common parameterization to faithfully represent the many streamlines within a single bundle, and to match different bundles. A straight-forward approach considers the natural grid of the image. This *voxel-based* approach often relies on registration of MRI or FA images prior to analysis. However, whole-brain registration does not guarantee an optimal alignment between corresponding fiber tracts due to large topological differences (Garyfallidis et al., 2015; O'Donnell and Pasternak, 2015; Yeatman et al., 2012).

An alternative approach focuses on specific bundles extracted from tractography. In this *tract-based* approach, fiber bundles are represented in a common coordinate system to enable a joint analysis of their properties (e.g., diffusion or geometric features). Many methods that perform along-tract analysis use arc-length (equi-distant) parametrization of individual streamlines to obtain a common representation (Yeatman et al., 2012; Colby et al., 2012; Corouge et al., 2006; Klein et al., 2007). Usually, a mean trajectory is constructed from corresponding points along the streamlines, to compactly represent different cross-sections of the bundle. In addition to equi-distant sampling, some methods aim to further refine the alignment across subjects, e.g., by excluding high variability areas such as the tracts' edges (Yeatman et al., 2012; O'Donnell et al., 2009), or incorporating anatomical landmarks to correct for spatial inconsistencies (Mårtensson et al., 2013). In (O'Donnell et al., 2009), inter-subject alignment is addressed by first registering FA images of all subjects, followed by selection of a representative (prototype) streamline for the entire group. Correspondence between all individual streamlines is then obtained by solving an optimal point match problem to the prototype streamline. A similar idea was suggested in (Wang et al., 2016), where a tractography atlas is used as a common inter-subject coordinate space by matching subjects' bundles to the atlas in a streamline-to-streamline manner.

A different paradigm considers parameterizations that are intrinsic to specific bundles. Yushkevich et al. (2008) used a parametric medial-surface representation of thin sheet-like fiber bundles, by projecting the volumetric data into a 2-manifold. In a similar manner, tube-like bundles were modeled by skeletons (centerlines) that represent their shape (Chung et al., 2010; Corouge et al., 2004). An extension of this approach was suggested in (Garyfallidis et al., 2012; Glozman et al., 2018), where the centerline is used for parcelling fiber bundles into local clusters that represent their geometry and are spatially consistent across subjects. Another recent method suggests using manifold learning to achieve joint parameterization of fiber bundles, by mapping corresponding tracts across subjects into a latent bundle core (Khatami et al., 2017).

The contribution of the proposed framework is two-fold, referring to both fiber bundle modeling and alignment. Aiming to perform quantitative *along-tract* analysis, we introduce the concept of *Fiber-Flux Diffusion Density* (FFDD) descriptors that combine the bundle's geometry with local diffusion measures. The geometry of the bundle is modeled by measuring its geometrical flux along different cross-sections of its trajectory, thus accounting for the local orientation and coherence of streamlines. By coupling this measure with DTI-derived scalars (e.g., FA), we create *along-tract profiles* that incorporate microscopic diffusion-related features as well as macrostructural geometry-related variations along tracts, which may not be reflected by either diffusion or geometrical features alone. Other related works have also accentuated the benefits in utilizing both micro- and macro-structural WM properties. For example (Zhang et al., 2010), presented a conjunctive analysis of FA measurements and bundle thickness, projected onto 2D skeletons of bundles to capture the effects of neurodegenerative disease on WM tracts. Similarly, along-tract analysis of diffusion parameters alongside geometrical measurements of bundles is proposed in (Mårtensson et al., 2013; Yendiki et al., 2011; Zhang et al., 2018). In this work, however, we suggest coupling geometrical and diffusion-based measures into one compact descriptor, rather than analyzing them separately, to allow for enhanced sensitivity to subtle changes in WM properties.

The task of fiber bundle alignment is addressed as a curve-matching problem between the mean trajectories of bundles. The proposed alignment method is based on an FFDD dissimilarity measure between tract profiles, thus utilizing both diffusional and geometrical information. This is in contrast to classical curve-matching algorithms, which rely exclusively on geometrical properties (e.g., arc-length and curvature) (Sebastian et al., 2003; Younes, 1998), and to purely FA-based registration methods (Andersson et al., 2007; Smith et al., 2006). Moreover, unlike traditional curve-matching approaches (Younes, 1998; Cohen et al., 1992), or other bundle alignment methods based on curve-matching (Prasad et al., 2014), we *do not* map one curve into another. Instead, we adapt the Fast Marching Method (FMM)[1] for curve alignment (Frenkel and Basri, 2003), to *symmetrically* match pairs of tracts with sub-voxel accuracy. This is accomplished by using the FFDD dissimilarity between the tracts as the inverse speed map of the FMM. The proposed alignment framework enables longitudinal and cross-sectional fiber bundles comparisons, and plays a key role in the construction of standardized (template) FFDD tract profiles across populations. These standardized profiles can be considered as tract-specific atlases, and facilitate group-wise statistical analysis for the assessment and localization of abnormalities in WM fiber tracts. Furthermore, we show that by applying the FMM to N-dimensional dissimilarity measures, a direct co-alignment of multiple bundles can be achieved in a single shot.

We demonstrate the advantages of the proposed FFDD fiber bundle modeling, alignment and variability analysis. A quantitative evaluation of the proposed alignment method, applied to Human Connectome Project (HCP) diffusion MRI dataset, demonstrates state-of-the-art performance in comparison to the well-established DTI-TK whole-brain registration algorithm (Zhang et al., 2006). We also show that the two approaches for FFDD alignment: the single-shot co-alignment of multiple bundles, and multiple pairwise alignments are both highly robust to different types of bundle deformations. We also demonstrate the proposed variability analysis framework in detection and localization of WM abnormalities, on two different datasets of contact-sport players. This includes an analysis of longitudinal scans of a basketball player with a *diagnosed* occipital mTBI and a frontal hemorrhage that can be identified in structural MRI; A group study comparing 13 active American-football players with possible (*undiagnosed*) mTBIs with 17 non-player control (NPC) subjects; and longitudinal analysis based on mid- and post scans of individual football players. Lastly, we show that the proposed FFDD method provides enhanced sensitivity to subtle structural anomalies in comparison to both along-tract FA analysis and geometry-based analysis alone.

A preliminary version of this work was presented in (Benou et al., 2018). Here we generalize the pairwise (2D) fiber tracts alignment method to accommodate N-dimensional co-alignment of multiple fiber tracts. We also provide a more thorough analysis using a much wider set of experiments with additional datasets. This includes an assessment of the proposed FFDD alignment on the HCP dataset; A comparison to the DTI-TK registration tool; A quantitative evaluation of the pairwise (2D) and generalized (N-dimensional) alignment techniques in the presence of different types of bundle deformations; And a group-wise longitudinal analysis of football players as well as the inclusion of three additional fiber tracts.

The rest of the paper is organized as follows: Section 2 presents the mathematical formulation for fiber bundles modeling, alignment, and statistical analysis using FFDD descriptors. In section 3 we present quantitative and qualitative evaluation of the FFDD alignment and variability analysis using cross-sectional and longitudinal data. A comprehensive discussion is provided in Section 4.

[1] The FMM was proposed by Sethian (1996) for solving boundary value problems of the Eikonal equation.

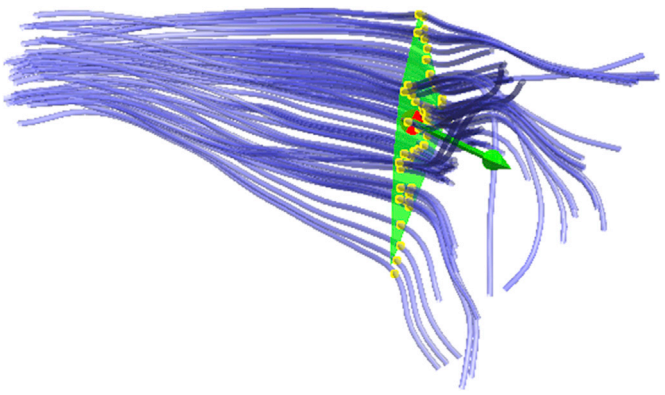

Fig. 1. FFDD illustration. Blue: fiber bundle B. Red: anchor point p. Green: cutting-plane π and its normal vector $\widehat{\boldsymbol{n}}_\pi(p)$. Yellow: intersection points $\{x_i\}$ to which the tangents $\{\widehat{\boldsymbol{\tau}}_i(x_i)\}$ and diffusion indices $\{S(x_i)\}$ are assigned.

2. Methods

The FFDD framework consists of the following stages: 1. *The FFDD descriptor*: a fiber bundle is described locally by combining its diffusion and geometry properties at a specific cross-section. 2. *Construction of along-tract profiles*: a full description of the bundle is obtained by repeating the FFDD computation along its mean trajectory, yielding an along-tract profile of FFDD measurements. 3. *Fiber bundle alignment*: Prior to quantitative analysis, fiber bundles are aligned according to their FFDD tract profiles. 4. *Along-tract variability analysis*: pairs of bundles are directly compared by the pointwise differences of their aligned FFDD profiles. Group-wise analysis is performed by computing pointwise statistics along a cohort of FFDD profiles.

2.1. Fiber-flux diffusion density descriptor

A fiber bundle B can be thought of as a set of similar trajectories with a common origin and destination, along which water molecules are diffused (Heimer, 2012). In the spirit of this notion, we define a local measure for quantifying the geometrical flux density of streamlines in bundle B through a plane π with normal $\widehat{\boldsymbol{n}}_\pi(p)$, for a given point $p \in \pi$, which we call the "anchor point" (see illustration in Fig. 1), i.e.,

$$F_B(\pi;p) = \frac{1}{N_p}\sum_{i=1}^{N_p} \widehat{\boldsymbol{\tau}}_i(x_i)\cdot\widehat{\boldsymbol{n}}_\pi(p), \tag{1}$$

where N_p is the number of intersected streamlines, $\xi = \{x_i\}$ is the set of intersection points between the plane and the fiber bundle, and $\{\widehat{\boldsymbol{\tau}}_i(x_i)\}$ are the tangents of the streamlines at those points. The plane π is oriented such that the flux density is maximized, i.e., $\widehat{\boldsymbol{n}}_\pi(p) = \underset{\widehat{n}_\pi}{\operatorname{argmax}} F_B(\pi;p)$. We use an iterative algorithm to solve this maximization problem in the spirit of (Tagliasacchi et al., 2009). The pseudo-code of this algorithm is given in Appendix A. We call $F_B(\pi;p)$ the fiber-flux density (FFD) of bundle B at point p. This measure quantifies the local geometric spread of streamlines in the bundle, such that areas with "incoherent" orientations are "punished" by having lower FFD values. We further introduce diffusion-related properties into our model by extending the FFD measure. Let $S(x_i)$ define a diffusion scalar of choice (FA, MD, AD, or RD) associated with the point x_i. We define the fiber-flux diffusion density (FFDD) as follows:

$$J_B(\pi;p) = \frac{1}{N_p}\sum_{i=1}^{N_p} S(x_i)\widehat{\boldsymbol{\tau}}_i(x_i)\cdot\widehat{\boldsymbol{n}}_\pi(p) \tag{2}$$

We obtain four FFDD descriptors, each couples a different diffusion scalar with local geometrical features of the bundle. Note that this coupling has a similar effect to wave interference. In other words, weighting the FFD by a diffusion scalar would amplify spatially consistent trends of the two measures (i.e., constructive interference), while restraining their contributions in case of spatial inconsistencies (destructive interference). This is a desired feature for variability analysis and anomaly detection, as it enhances sensitivity when the two measures "agree", while maintaining specificity due to the restraining effect. Finally, we refer to the FFDD as a vector $\boldsymbol{J}_B(p) = J_B(p)\widehat{\boldsymbol{n}}(p)$ to further account for the local orientation of the fiber bundle.

2.2. Along-tract FFDD profiles

For a complete along-tract representation of the bundle, we wish to obtain a representative path along which FFDD measurements will be taken (i.e., a trajectory of "anchor points"). We refer to this path as the "mean streamline" of the bundle throughout the rest of the paper. We calculate the mean streamline using an algorithm based on Fourier descriptors (Chung et al., 2010). According to this method, individual tractography streamlines are represented by the coefficients of their cosine series expansions, computed using a least squares estimation. The mean streamline is then optimally obtained by averaging the representation coefficients of all streamlines, and applying the inverse transformation. We represent the resulting mean streamline using arc-length parametrization, i.e., $c(s) = (x(s), y(s), z(s))$, where s is its arc-length parameter. *Along-tract profiles* are obtained by applying the FFDD descriptor at M equally distributed "anchor points" along the mean streamline, i. e, $\{\boldsymbol{J}_B(p_m)\}_m$; $\{p_m\} = \{c(s^m)\}_{m=1}^M$. Throughout this work we use $M = 100$ points, unless stated otherwise.

2.3. Fiber bundles alignment

We address the alignment of two bundles B_1 and B_2 as a curve-matching problem between their streamlines $c_1(s_1)$ and $c_2(s_2)$, where $s_1 \in [0\ ,\ L_1]$ and $s_2 \in [0\ ,\ L_2]$ are the respective arc-length parameterizations. We adapt the FMM-based symmetrical curve-matching framework of (Frenkel and Basri, 2003), allowing for alignment to be achieved in a

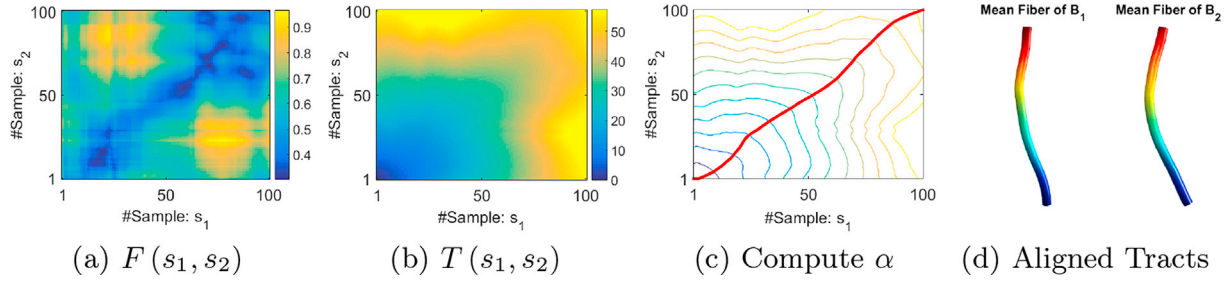

Fig. 2. Alignment using FMM. (a) Local dissimilarities $F(s_1, s_2)$ based on FFDD profiles. (b) $T(s_1, s_2)$ obtained by solving the Eikonal equation. (c) The alignment path $\alpha(\tau)$ computed by backtracking along the gradients of $T(s_1, s_2)$. (d) The resulting alignment, color-coded along the mean streamlines of the bundles. Identical colors correspond to homologous points.

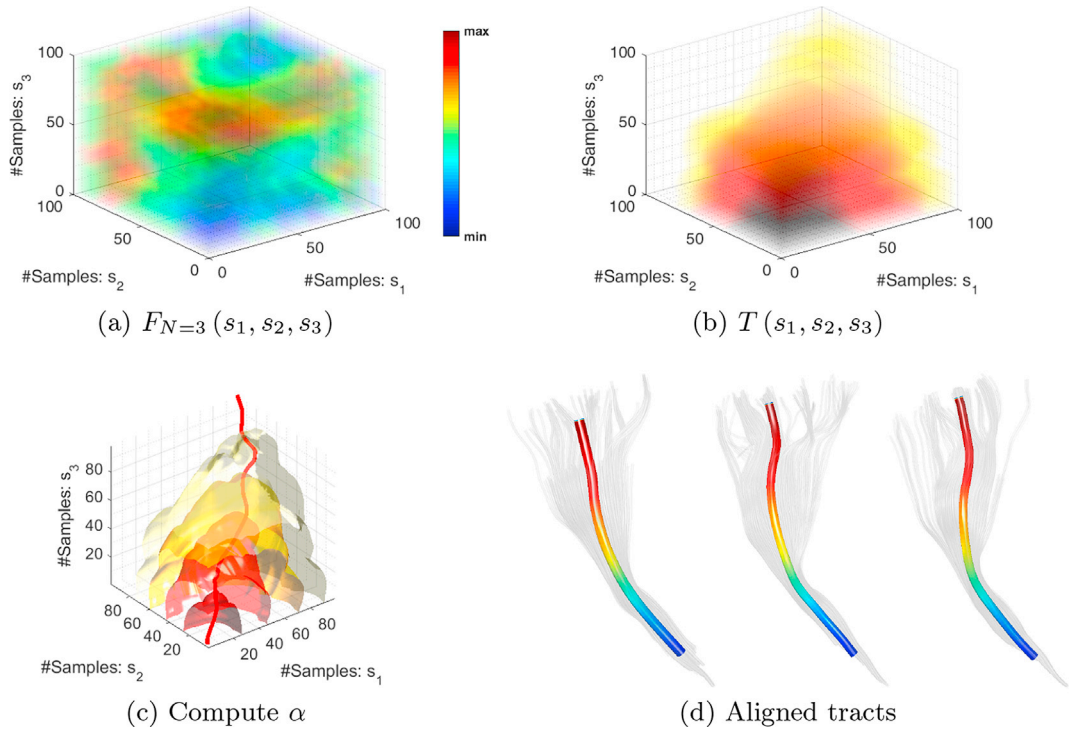

Fig. 3. Single-shot co-alignment of three fiber bundles using FMM. (a) 3D local dissimilarity map $F_{N=3}(s_1, s_2, s_3)$ based on the tracts' FFDD profiles. (b) The weighted distance matrix $T(s_1, s_2, s_3)$ obtained by solving the Eikonal equation. (c) The alignment path $\alpha(\tau)$ computed by backtracking along the gradients of $T(s_1, s_2, s_3)$. (d) The resulting alignment, color-coded along the mean streamlines of the tracts. Identical colors correspond to homologous points.

Table 1
Average alignment scores ± std of FFDD and DTI-TK (higher is better).

Criterion	Method	Left CST	Right CST	Left IFOF	Right IFOF	Fminor
FA-based	FFDD	**0.846** ±0.093	**0.894** ±0.074	**0.702** ±0.121	**0.692** ±0.094	**0.912** ±0.043
	DTI-TK	0.694 ± 0.256	0.791 ± 0.116	0.542 ± 0.211	0.588 ± 0.218	0.892 ± 0.041
Tensor-based	FFDD	**0.979** ± 0.007	**0.981** ± 0.016	**0.828** ± 0.077	0.792 ± 0.047	0.884 ± 0.045
	DTI-TK	0.969 ± 0.023	0.977 ± 0.011	0.826 ± 0.077	**0.803** ± 0.065	**0.897** ± 0.046

sub-sampling resolution. Nevertheless, rather than using geometrical properties alone for the construction of the inverse speed map $F(s_1, s_2)$, we propose a new dissimilarity measure that relies on the FFDD profiles:

$$F(s_1, s_2) = \|\boldsymbol{J}_{B_1}(c_1(s_1)) - \boldsymbol{J}_{B_2}(c_2(s_2))\| + \lambda \tag{3}$$

where λ is a scalar used for regularization set as in (Frenkel and Basri, 2003). Given $F(s_1, s_2)$, the FMM solves the Eikonal equation $|\nabla T(s_1, s_2)| = F(s_1, s_2)\ \forall\, s_1, s_2$, providing as output the weighted distance matrix $T(s_1, s_2)$. Fig. 2a–b illustrate $F(s_1, s_2)$ and $T(s_1, s_2)$, respectively. The optimal alignment is then defined by the shortest path in $F(s_1, s_2)$ from the starting point $(0, 0)$ to the endpoint (L_1, L_2). The alignment path $\alpha(\tau) = (s_1(\tau), s_2(\tau))$ defines pairs of matching points between the bundles, and is computed with sub-voxel resolution as follows:

$$\alpha(\tau - \varepsilon) = \alpha(\tau) - \varepsilon \nabla T(s_1, s_2)\ ;\ \alpha(L) = (L_1, L_2) \tag{4}$$

As illustrated in Fig. 2c. The step size ε is usually set to some small value ($\varepsilon \ll 1$) For uniformity, we re-sample α into M samples, i.e., $\{\alpha(\tau^m)\}_{m=1}^{M}$, such that the aligned mean streamlines are obtained by $\tilde{C}_1 = \{c_1(s_1(\tau^m))\}_{m=1}^{M}$ and $\tilde{C}_2 = \{c_2(s_2(\tau^m))\}_{m=1}^{M}$ (see Fig. 2d), and their tract profiles are aligned accordingly: $\tilde{J}_{B_1} = \{\boldsymbol{J}_{B_1}(c_1(s_1(\tau^m)))\}_{m=1}^{M}$ and $\tilde{J}_{B_2} = \{\boldsymbol{J}_{B_2}(c_2(s_2(\tau^m)))\}_{m=1}^{M}$.

2.4. Along-tract variability analysis

Pairwise Comparison: Let $\tilde{J}_{B_1}$ and $\tilde{J}_{B_2}$ be a pair of aligned tract profiles to be compared, e.g., of a subject-specific tract in two longitudinal scans. We define a pointwise dissimilarity measure between them as follows:

$$d_J(B_1, B_2; \alpha(\tau^m)) = \|\boldsymbol{J}_{B_1}(c_1(s_1(\tau^m))) - \boldsymbol{J}_{B_2}(c_2(s_2(\tau^m)))\| \tag{5}$$

Although we focus here on computing local dissimilarities along the two bundles, global dissimilarity can also be calculated: $D_J(B_1, B_2) = \int_{\alpha} d_J(B_1, B_2; \alpha(\tau)) d\alpha$.

Group-Wise Analysis: Quantitative evaluation of multiple subjects, for either intra-group or inter-group analysis, is facilitated as follows:

Aligning multiple bundles: Analyzing a group of subjects requires the alignment of multiple fiber bundles. This can be performed iteratively, using multiple pairwise alignments. Let $J_g = \{\boldsymbol{J}_{B_n}(c_n(s))\}_{n=1}^{N_g}$ denote the set of N_g tract profiles of a group of subjects, and let $C_g = \{c_n(s)\}_{n=1}^{N_g}$ denote their respective mean streamlines with a joint arc-length parameterization s. We define a *reference* tract profile, with its corresponding mean streamline, as follows:

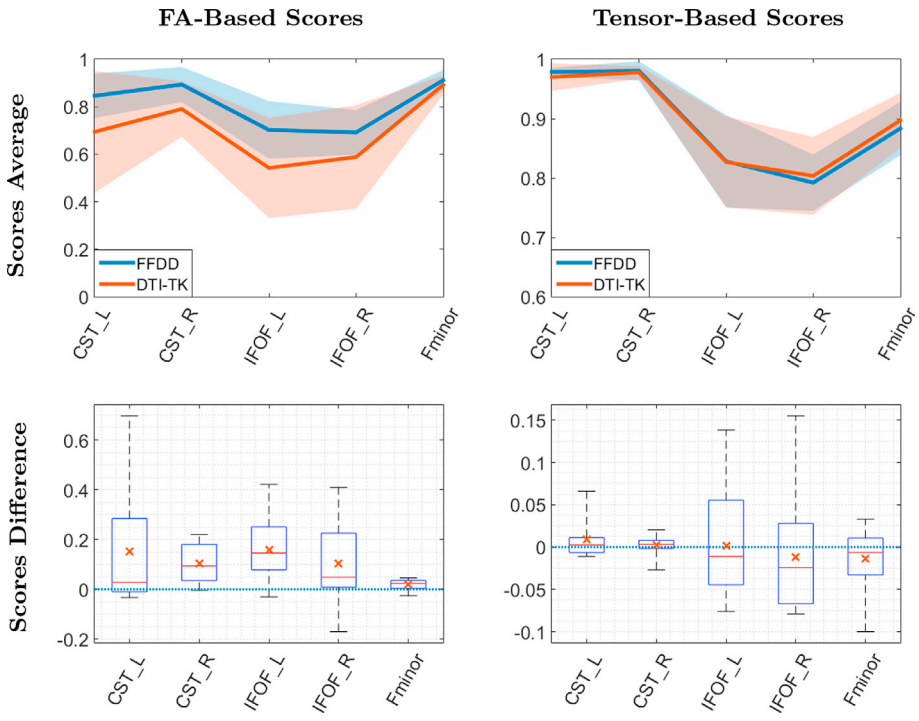

Fig. 4. Comparison to DTI-TK whole-brain registration. Top: Average FA- and tensor-based alignment scores for the five examined bundles across 12 subject pairs. The plot shows the mean scores across all 12 pairs (bold lines), where the shaded regions cover ± 1 std. The colors red and blue are used for DTI-TK and FFDD, respectively. Bottom row: Box-plot of the differences in FA- and tensor-based alignment scores between FFDD and DTI-TK. The red line in each box represents the median difference, the red '**x**' represents the mean, the edges of the boxes are the 25th and 75th percentiles, and the whiskers extend to the min and max values. Positive difference values (above the dashed line) indicate that FFDD performed better than DTI-TK.

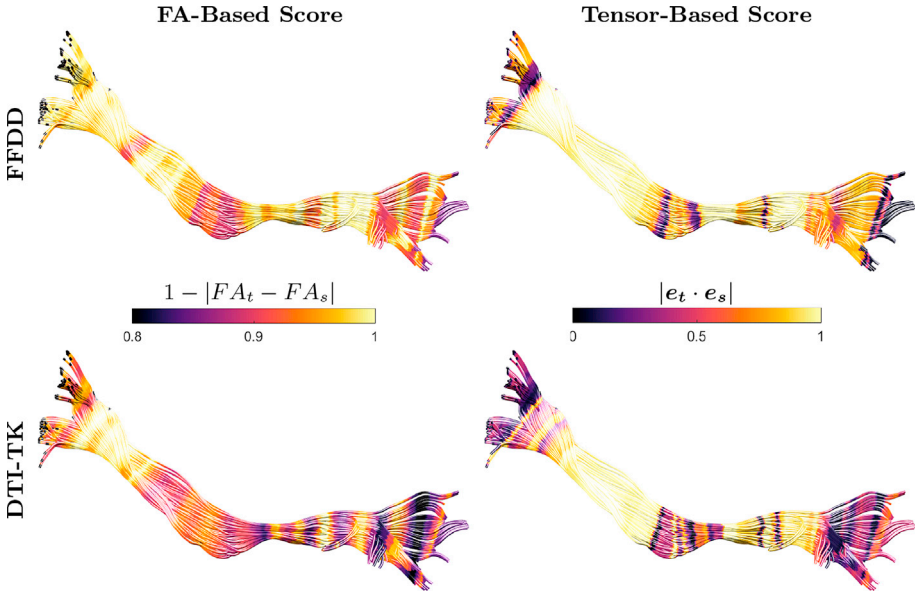

Fig. 5. Alignment scores example. FA- and tensor-based alignment scores obtained by FFDD and DTI-TK, color-coded along the IFOF of one of the template subjects. The scores are averaged along planar cross-sections of the bundle in order for the visualization to be comparable between the two methods. Notice that the proposed FFDD method achieves better alignment scores near the terminals of the bundle, where accurate alignment is challenging due to large topological differences across subjects.

$$\boldsymbol{J}_{ref}(s)=\frac{1}{N_g}\sum_{n=1}^{N_g}\boldsymbol{J}_{B_n}(c_n(s)) \quad , \quad C_{ref}(s)=\frac{1}{N_g}\sum_{n=1}^{N_g}c_n(s). \tag{6}$$

Alignment of the tract profiles is obtained by first mapping each of them to the reference tract as described in section 2.3. We then interpolate the resulting alignment paths $\{\alpha_n(\tau)\}_{n=1}^{N_g}$ such that they all contain the same set of M samples of the reference tract $\{c_{ref}(s^m)\}_{m=1}^{M}$.

Creating a group template: We construct an FFDD *bundle-specific atlas* of a group by pointwise averaging all of the aligned tract profiles. This atlas represents the *group-mean* FFDD tract profile, which we will sometimes refer to as the *standardized* profile of the group. By also computing the pointwise standard deviation (std) of the aligned profiles, we can obtain a statistical representation of how FFDD values vary within the group, along the tracts. For example, when applied to a cohort of control subjects, the atlas of FFDD values can be used as a reference for evaluating test subjects.

Group-wise comparisons are facilitated by aligning all FFDD profiles to a common coordinate system. For comparing between test and control groups, tract profiles of all individual test subjects are aligned to the control group atlas. Then, their mean tract profile and pointwise std are computed.

Statistical analysis: We follow the commonly used approach in TBI detection, aiming to identify "out-of-the-normal" statistics in patients with respect to a normal control group atlas (Shenton et al., 2012; Bouix et al., 2013). For evaluation of a single test subject, we present a z-score at each point along its FFDD tract profile with respect to the control group-mean profile and std. For cross-sectional experiments (e.g., comparing test and control groups), we perform an unpaired

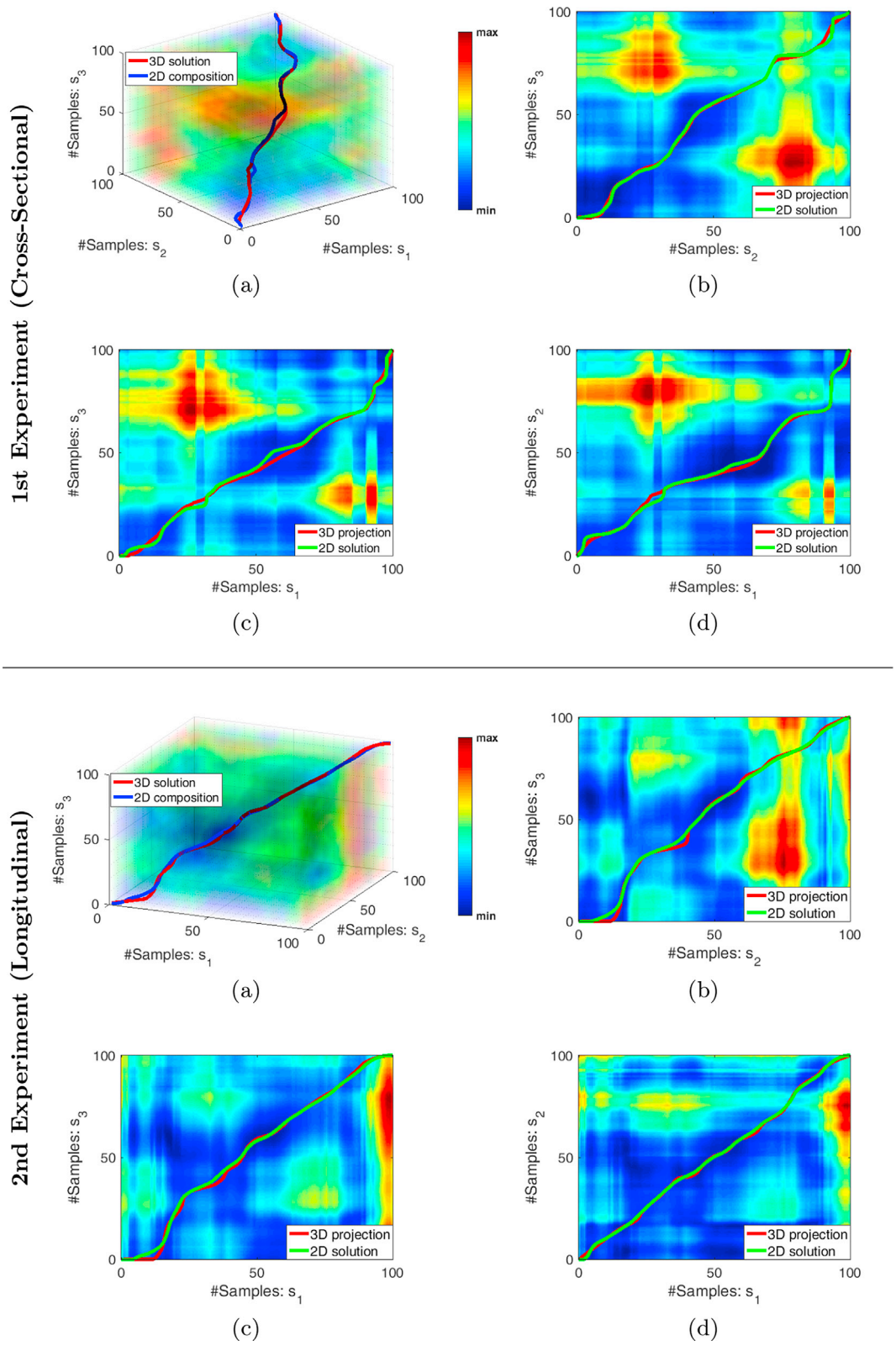

Fig. 6. Qualitative comparison between single-shot co-alignment and composition of pairwise alignments, for the cross-sectional (top panel) and longitudinal (bottom panel) experiments. (a) The 3D single-shot alignment path $\alpha(\tau)$ and the pairwise-composite alignment path $\alpha_{comp}(\tau)$, plotted on $F_{N=3}(s_1, s_2, s_3)$. (b) The (s_2, s_3) projection of $\alpha(\tau)$ and the pairwise (2D) alignment path $\alpha_{23}(\tau)$, plotted on $F_{N=3}(s_1, s_2, s_3)$ marginalized along s_1. (c) The (s_1, s_3) projection of $\alpha(\tau)$ and the pairwise (2D) alignment path $\alpha_{13}(\tau)$, plotted on $F_{N=3}(s_1, s_2, s_3)$ marginalized along s_2. (d) The (s_1, s_2) projection of $\alpha(\tau)$ and the pairwise (2D) alignment path $\alpha_{12}(\tau)$, plotted on $F_{N=3}(s_1, s_2, s_3)$ marginalized along s_3.

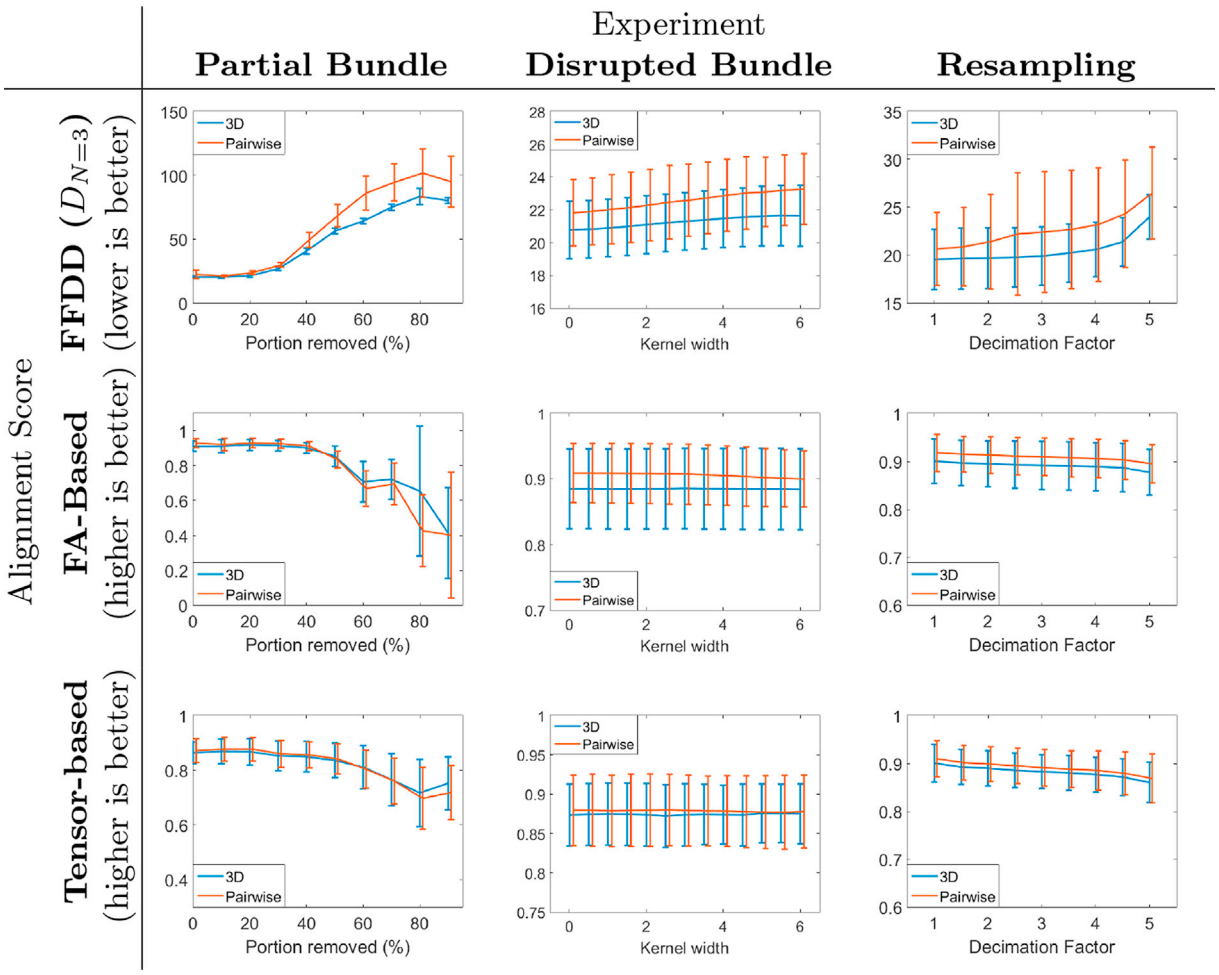

Fig. 7. Quantitative comparison between pairwise and single-shot alignments. From left to right: three different bundle deformation experiments. From top to bottom: three different alignment quality scores. Each plot shows the mean and std of the alignment score across all 6 bundle triplets.

(two-sample) T-test at each point along the FFDD tract profiles of test and control subjects. To correct for multiple comparisons along the tract, the resulting p-values are adjusted using the false discovery rate (FDR) method (Benjamini and Hochberg, 1995). Similarly, for a longitudinal study of a test group (e.g., comparing two different time points) we perform paired (one-sample) T-tests along the tract profiles, followed by FDR correction.

2.5. Single-shot alignment of multiple fiber bundles

The FMM-based alignment framework described in section 2.3 can be extended beyond pairwise bundle matching to allow a direct co-alignment of multiple fiber bundles. Let us consider a set of $N > 2$ fiber bundles to be aligned, $\{B_n\}_{n=1}^{N}$, with their corresponding mean streamlines $\{c_n(s_n)\}_{n=1}^{N}$ and FFDD tract profiles $\{\boldsymbol{J}_{B_n}(c_n(s_n))\}_{n=1}^{N}$. To support the joint alignment of N fiber bundles, we generalize the pairwise dissimilarity measure in Eq. (3) as follows:

$$F_N(s_1,\ldots,s_N) = \sum_{i=1}^{N-1}\sum_{j=i+1}^{N} \left\| \boldsymbol{J}_{B_i}(c_i(s_i)) - \boldsymbol{J}_{B_j}(c_j(s_j)) \right\| + \lambda \tag{7}$$

Note that F_N is a summation over all possible combinations of the pairwise dissimilarity measure $F_{N=2}$. As in the pairwise alignment case, we aim to incorporate this dissimilarity measure into the FMM framework. Therefore, the N-dimensional function $F_N(s_1,\ldots,s_N)$ is used as an inverse speed map in the N-dimensional Eikonal equation i.e., $|T(\boldsymbol{s})| = \nabla F_N(\boldsymbol{s})\ ;\ \boldsymbol{s} = (s_1,\ldots,s_N)$. Accordingly, the optimal alignment of all N fiber bundles is given by the shortest path in $F_N(\boldsymbol{s})$ from $\boldsymbol{s} = (0,\ldots,0)$ to $\boldsymbol{s} = (L_1,\ldots,L_N)$, defining a curve embedded in $\mathbb{R}^N$ i.e., $\alpha(\tau) = (s_1(\tau),\ldots,s_N(\tau))$. Given the weighted distance matrix $T(\boldsymbol{s})$, the optimal alignment path is computed by backtracking along the gradients of $T(\boldsymbol{s})$, extending Eq. (4) to N-dimensions. Finally, the optimal path $\alpha(\tau)$ is resampled into M equidistant points such that the aligned FFDD tract profiles are given by $\{\boldsymbol{J}_{B_n}(\alpha^{(n)}(\tau^m))\}_{m=1}^{M}\ \forall\, n = 1,\ldots,N$, where $\alpha^{(n)}$ denotes the n-th component of $\alpha(\tau)$. Fig. 3 demonstrates the different stages of this alignment process. We note that the proposed method enables a single-shot solution to the co-alignment problem of multiple fiber bundles. This is in contrast to the common co-alignment approach in which all individuals are iteratively aligned to their average until convergence. Moreover, the proposed single-shot optimization provides an exact solution to the N-dimensional co-alignment problem, while the iterative approach only provides an approximation.

3. Experiments and results

In the following sections we demonstrate and evaluate the proposed FFDD tract-specific modeling, alignment and variability analysis. Data and preprocessing are presented in Section 3.1. Section 3.2 presents a comparison of the proposed FFDD alignment method with the commonly used DTI-TK whole-brain registration algorithm (Zhang et al., 2006). In Section 3.3 we demonstrate the FFDD single-shot algorithm for simultaneous alignment of multiple fiber tracts. We also show that both pairwise and single-shot FFDD alignment algorithms are robust to different types of bundle deformations. FFDD variability analysis is first assessed in

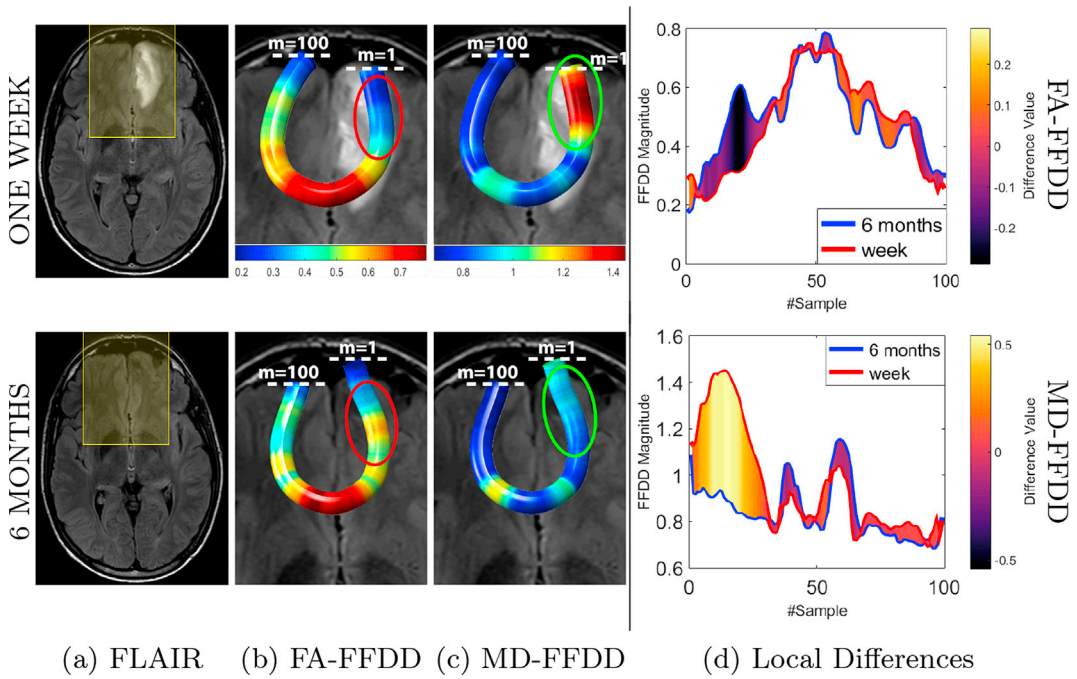

Fig. 8. Longitudinal analysis along the Fminor tract of the basketball player. **Left Panel:** (a) FLAIR scans (axial slices), one week post-injury (**top**) and 6 months post-injury (**bottom**). The area around the hemorrhagic contusion is highlighted in yellow boxes. Notice that the lesion is no longer visible 6 months after the injury. In (b) and (c) the tracts are colored-coded by the magnitude of their FFDD profiles. Regions with large longitudinal changes (marked in red and green ellipses) correspond to the lesion area. **Right Panel:** (d) FA- and MD-FFDD tract profiles of both scans. Pointwise differences between the tract profiles are color-coded on the graph.

Section 3.4 using longitudinal scans of a basketball player with diagnosed TBI. In Section 3.5 we present longitudinal and cross-sectional analysis of football players data. A comparison with standard along-tract approaches is presented in Section 3.6.

3.1. Data and pre-processing

We used the Human Connectome Project (HCP) adult diffusion MRI dataset (Fan et al., 2016) for the bundle alignment experiments (Section 3.2-3.3). DTI tensor reconstruction was performed using FSL's DTIFIT.

We conducted the variability analysis (Section 3.4-3.6) using two datasets of contact-sports players, and an additional non-player controls (NPC) dataset. The NPC group includes scans of healthy age-matched males. Diffusion weighted images (DWI) of all subjects were acquired on a 3T Philips Ingenia scanner using a single-shot, spin-echo, echo-planar imaging (EPI) sequence (TE = 106 ms, TR = 9000 ms, FOV = $224 \times 224 \times 120$ mm). A total of 60 2 [mm]-thick slices were acquired with 33 different gradient directions (b = 1000 s/mm^2) with a voxel resolution of $1.75 \times 1.75 \times 2$ mm. Pre-processing of DWIs was performed using DSI Studio (http://dsi-studio.labsolver.org/), and included motion and eddy currents correction, as well as rigid alignment of subjects' B0 (non-diffusion weighted) images to the SPM MNI T1-template. The gradient vectors were rotated accordingly. DTI tensor reconstruction was then performed according to (Jiang et al., 2006).

In all experiments (alignment and variability analysis) tractography was performed using DSI studio's deterministic streamline tracking (Yeh et al., 2013). Tracking parameters were set as follows: The FA threshold was set to 0.2, the angular threshold to 70°, step size was 1 mm, and streamlines longer than 300 mm or shorter than 30 mm were discarded. Seeding was performed by placing 20,000 random points within the entire white matter volume. Fiber bundles were extracted by placing multiple regions of interest (ROIs) from the Johns Hopkins University (JHU) WM atlas labels (Mori et al., 2008). The ROIs were automatically placed using DSI Studio's built-in function, which aligns subjects' FA scans and the JHU atlas in a two-step process (an initial affine transformation followed by a diffeomorphic mapping) for maximizing mutual information. Eight major fiber bundles were extracted: the left and right inferior fronto-occipital fasciculus (IFOF), left and right inferior longitudinal fasciculus (ILF), left and right corticospinal tract (CST), and the forceps minor (Fminor) and forceps major (Fmajor) tracts. We chose to analyze these specific tracts since they commonly present abnormalities in mTBI studies (Hulkower et al., 2013), and have been shown to be susceptible to sports-related head trauma (Bigler, 2018).

3.2. Alignment quality assessment

DTI registration algorithms can be broadly divided into three categories: scalar map-based, tensor-based, and tractography-based. In its essence, FFDD alignment is a tractography-based technique since it is applied directly to fiber bundles. However, rather than solely matching the structure or shape of tractograms as in typical tractography registration algorithms (Garyfallidis et al., 2015; O'Donnell et al., 2012; Olivetti et al., 2016; Zvitia et al., 2010), it also utilizes diffusion measurements along the tract (FA, MD, etc.), such that diffusion-related correspondence is also obtained as in scalar image-based registration (Andersson et al., 2007). Furthermore, since the FFDD alignment metric incorporates the local orientation of fiber bundles, it implicitly aligns the underlying tensor orientation as in tensor-based algorithms (Zhang et al., 2006; Yap et al., 2009; Yeo et al., 2009). Therefore, the FFDD alignment methodology presented in this work embraces desirable qualities from each of these categories.

To evaluate the alignment quality of the proposed FFDD method, we compare its performance to the well-known DTI-TK whole-brain registration algorithm (Zhang et al., 2006). While there exist various DTI registration tools, DTI-TK has shown to achieve state-of-the-art results in several evaluation studies (Wang et al., 2011, 2017) and therefore is a good performance benchmark.

Experimental Setup: For this experiment we used the Human Connectome Project (HCP) adult diffusion MRI dataset (Fan et al., 2016). In order to avoid bias and/or differences in image characteristics between

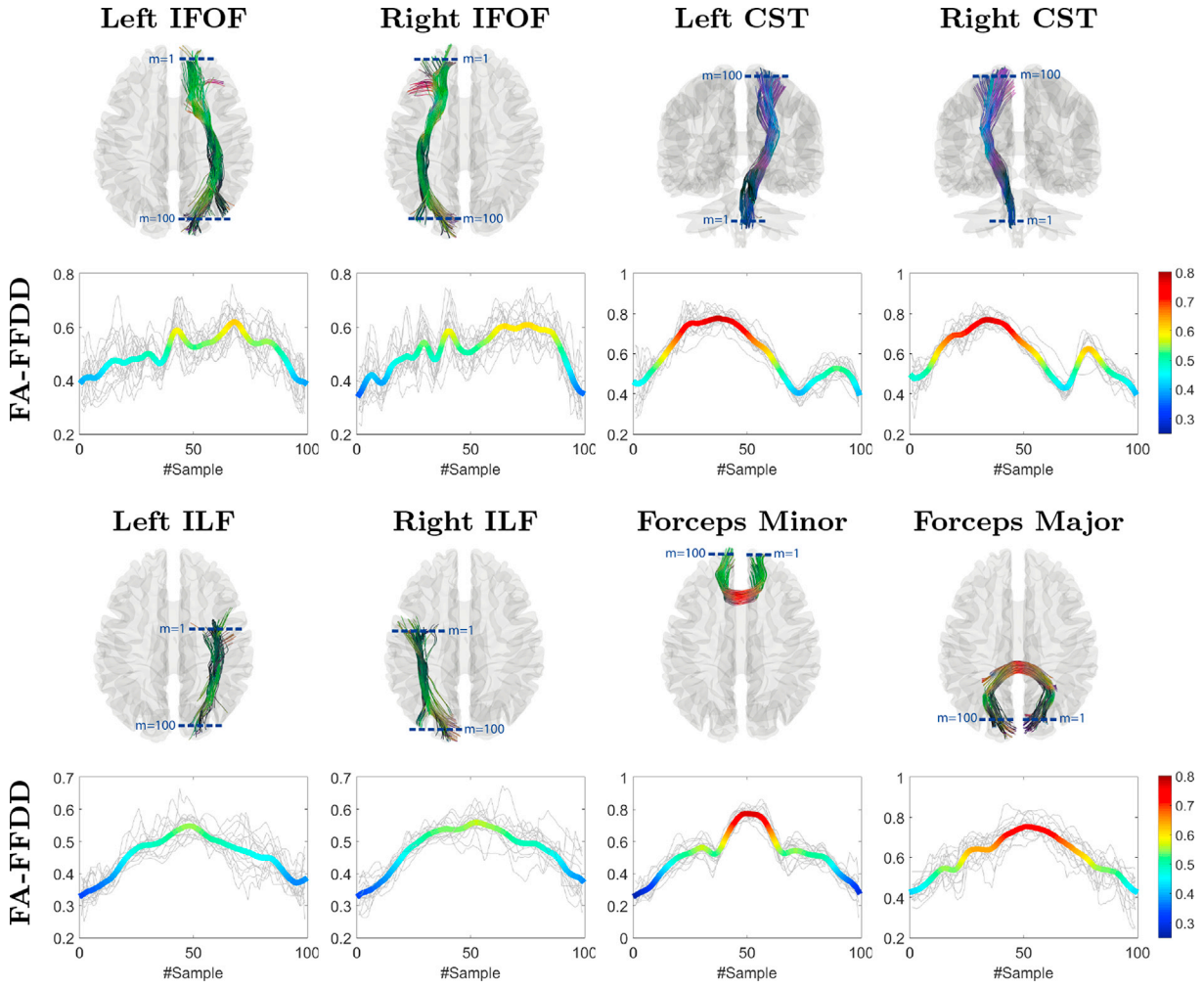

Fig. 9. 1st and 3rd rows: The eight examined fiber tracts colored by their orientation. **2nd and 4th rows**: Their standardized FA-FFDD tract profiles colored by their magnitude, constructed from the aligned tract profiles of control subjects (in gray).

individual subjects and a group-mean template, registration was evaluated on a subject-to-subject basis as suggested by (Wang et al., 2017; de Groot et al., 2013). However, while in (Wang et al., 2017) all subjects are aligned to the same reference subject, in (de Groot et al., 2013) pairs of subjects are compared. Using a similar methodology to (de Groot et al., 2013), we consider 12 randomly selected pairs of subjects from the HCP dataset on which registration is evaluated. One subject from each pair was then selected as the "target" and the other as the "source" for the alignment. We note that since DTI-TK is a tensor-based registration algorithm, whereas FFDD alignment is tractography-based, the order of tractography and registration operations is different for each method: When evaluating the FFDD method, tractography and fiber bundles extraction are first performed in the native space of each subject, prior to alignment. Then, FA-FFDD profiles of each pair are computed and aligned as described in Sections 2.2 and 2.3. In contrast, when evaluating the DTI-TK method, DTI images of "source" subjects are first registered to the "targets", followed by tractography and fiber bundle extraction. For both methods, the evaluation included five major fiber tracts: the left and right IFOF, left and right CST, and the Fminor. Tractography and bundles extraction were performed using DSI-studio as described in Section 3.1.

Evaluation Metrics: For quantitative evaluation, two different DTI-based matching criteria were used, similar to those suggested in (Wang et al., 2011). The first criterion is based on the goodness of fit between diffusion parameters along the two aligned fiber tracts. Specifically, it measures the correlation coefficient between the FA curves (profiles) of the target and source subjects after alignment. The second criterion measures the level of agreement between the principal tensor orientations of the source and target subjects. This criterion is defined[2] for each pair of corresponding points as follows $S_{t,s}(i) = \left|\mathbf{e_t}(\mathbf{i}) \cdot \mathbf{e_s}(\mathbf{i})\right|$, where $\boldsymbol{e_s}$ and $\boldsymbol{e_t}$ are the principal eigenvectors of the source and target subjects, respectively. The total registration score for a given pair of bundles is then obtained by averaging this measure over all N_r corresponding points of the bundles, i.e., $\overline{S}_{t,s} = \frac{1}{N_r}\sum_{i=1}^{N_r} S_{t,s}(i)$.

Results: The comparison of alignment quality between DTI-TK and FFDD is shown in Table 1 and Fig. 4. The scores represent the average performance in FA- and tensor-based criteria over all 12 pairs of subjects, and are presented for each tract individually. Results show that for the FA-based criterion, FFDD alignment outperforms DTI-TK in all of the five examined tracts. In Appendix E of the supplementary material we show that these performance differences are statistically significant. For the tensor-based criterion, our FFDD method demonstrated comparable results with DTI-TK, achieving a higher mean score in three out of the five examined tracts, even though DTI-TK directly operates on the tensor images of subjects. We note that FFDD alignment scores also present lower standard deviation in most cases, indicating improved robustness in aligning areas with high dissimilarity between subjects. This is visually demonstrated in Fig. 5, showing an example of the alignment accuracy of the two methods along the IFOF. Notice that for both FA- and tensor-

[2] We note that unlike (Wang et al., 2011) we did not weight each dot product with the target's FA values to avoid biased results.

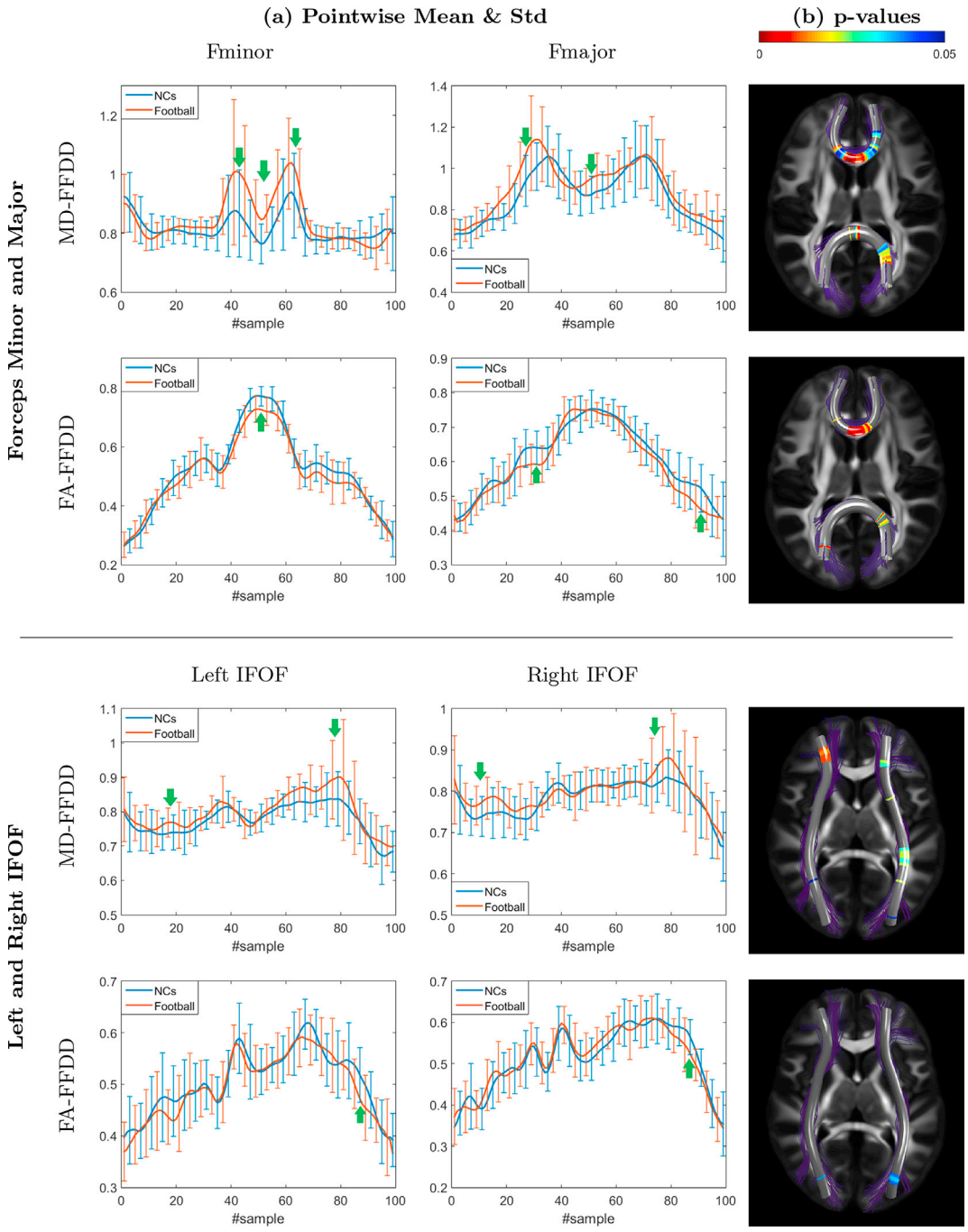

Fig. 10. FFDD statistical analysis of the football and NPC groups. FA- and MD-FFDD profiles of football players were aligned to the standardized FA- and MD-FFDD profiles of NPCs, respectively. (a) The group-mean tract profiles along the Fminor and Fmajor (top panel) and the left and right IFOF (bottom panel). The error bars represent ± one std from the mean profile. Areas of statistically significant differences are marked with green arrows. (b) P-values (corrected for multiple comparisons using FDR), color-coded along the tracts. Statistically significant differences (p-value<0.05) between football and NPC groups are mostly demonstrated around the center of the Fminor and Fmajor, and near the edges of the left and right IFOF.

based criteria, FFDD achieves a more accurate alignment near the edges of the tract, where the inter-subject variability is larger.

3.3. *Comparing single-shot with multiple pairwise alignments*

Qualitative Comparison: We next demonstrate our method for single-shot co-alignment of multiple tracts, presented in section 2.5, for the case of N = 3. We perform two experiments: (a) Cross-sectional co-alignment of three CST bundles of randomly selected subjects from the HCP diffusion MRI dataset (see appendix Fig. F1a). (b) Longitudinal co-alignment of the Fminor tract extracted from mid-season and post-season scans of a single player from our football dataset, with the computed FFDD atlas of the NPC group for the Fminor tract (see appendix Fig. F1b). In both experiments, we compared the single-shot co-alignment with the results obtained by multiple pairwise bundle alignments. For the purpose of this comparison, the pairwise alignment of each of the three possible pairings were computed, i.e., (B_1, B_2), (B_1, B_3), and (B_2, B_3). We denote their respective planar alignment paths by $\alpha_{12}(\tau)$, $\alpha_{13}(\tau)$, and $\alpha_{23}(\tau)$.

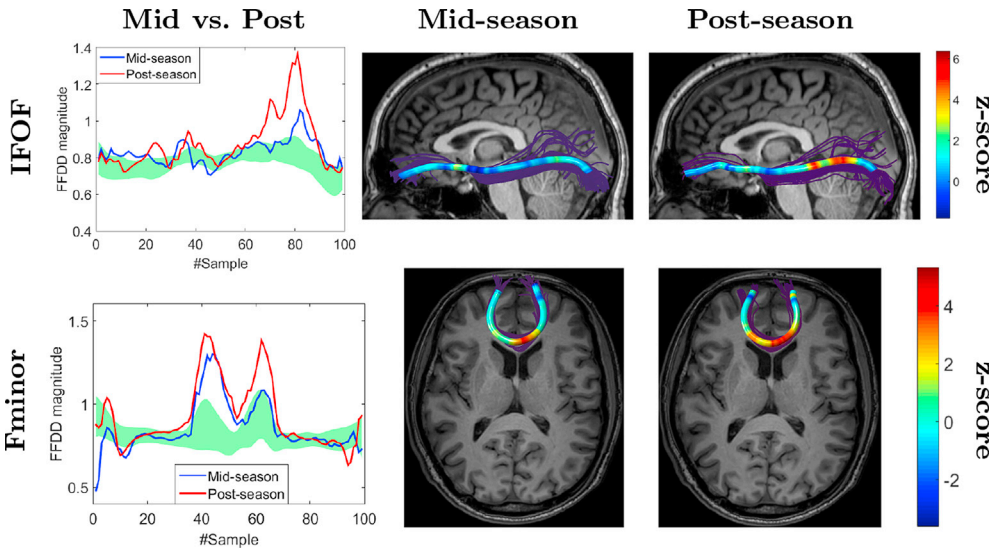

Fig. 11. Longitudinal changes in FFDD values along the IFOF (top) and Fminor (bottom) tracts of two football players. **Left:** Mid- and post-season MD-FFDD tract profiles of the player. The green region represents ±1 std from the NPC group-mean profile. The players' profiles were aligned to the group-mean MD-FFDD profile of the NPC group. **Middle and Right:** Z-scores of the mid- and post-season profiles, color-coded along the tract. Note that in both cases the post-season profile demonstrates aggravation in magnitude and spatial extent of the abnormality compared to mid-season.

These paths can be considered as 2D projections on different planes of the (s_1, s_2, s_3) space. We therefore compose these projections into a single 3D alignment path given by $\alpha_{comp}(\tau) = (\alpha_{12}^{(1)}(\tau), \alpha_{23}^{(1)}(\tau), \alpha_{13}^{(2)}(\tau))$, where $\alpha_{ij}^{(k)}$ denotes the k-th component of α_{ij}. The differences between the resulting pairwise-composite alignment $\alpha_{comp}(\tau)$ and the 3D single-shot solution $\alpha(\tau)$ are presented for the two experiments in Fig. 6. Fig. 6a shows a 3D visualization of the comparison, and Fig. 6b–d presents different 2D projections. For example, Fig. 6c presents the pairwise alignment $\alpha_{13}(\tau)$ and the projection of the single-shot 3D alignment on the (s_1, s_3) plane. The two paths are plotted on the marginalization of $F_{N=3}$ along the s_2 axis, i.e., $\int_0^{L_1} F_{N=3}(s_1, s_2, s_3)ds_2$. These results demonstrate that the pairwise-composite alignment yields a similar, but not identical, solution to the single-shot co-alignment. This implies that composition of several pairwise-optimal alignments does not necessarily yield a globally optimal co-alignment of multiple bundles (in terms of F_N).

Quantitative Comparison: To better understand the practical differences between the pairwise and single-shot approaches, we conducted three quantitative experiments comparing their performance under different bundle deformations:

1. *Partial bundle*: in this experiment, a segment was removed from one of the bundles, starting from the endpoint and gradually extending up to 90% of the original bundle.
2. *Disrupted bundle*: in this experiment we assessed the alignment performance in the presence of a simulated focal injury, located at the center of one of the bundles. Since such an injury is likely to decrease both FA and FFD values around the injured area, it was simulated by pointwise multiplying the FA-FFDD profile of the bundle by an exponential "disruption-kernel" $w(s) = 1 - A\exp\left(-\frac{(s-f)^2}{2\sigma^2}\right)$, where the amplitude was set to $A = 0.8$, the center of the window was set to $f = 50$, and the kernel width varied from $\sigma = 0$ (no disruption) to $\sigma = 6$.
3. *Resampling*: in this experiment we tested the sensitivity of the two approaches to different sampling step sizes of the bundles. This was performed by gradually down-sampling the FFDD profiles of all bundles to be aligned, starting from a decimation factor of 1 (100 equi-distant samples, no down-sampling) up to a decimation factor of 5 (20 equi-distant samples, i.e., the step size is 5-times larger).

The three experiments were performed on the Fminor bundle of six different triplets of randomly selected subjects from the HCP dataset. The alignment was based on the FA-FFDD profiles of the bundles, where each triplet was aligned twice - once using the pairwise composite approach, and once using the 3D single-shot approach. The resulting alignments were then assessed using three different matching criteria:

1. Total FFDD dissimilarity after alignment, given by $D_{N=3} = \int_\alpha F_{N=3}(s_1, s_2, s_3)d\alpha$. Notice that this score is calculated once for a given triplet of bundles, and reflects the overall FFDD "disagreement" between them (lower is better).
2. The FA-based correlation criterion, as described in section 3.5. Notice that this a pairwise score, which is calculated separately for each pair of aligned bundles (i.e., three times for a given triplet), and reflects the goodness of FA fit for a specific pair (higher is better).
3. The tensor-based criterion, as described in section 3.5. This score is also calculated individually for each pair, and reflects the level of agreement between tensor directions for a specific pair (higher is better).

For each experiment, the average alignment score and its std were computed over all six triplets of bundles. Results are summarized in Fig. 7. Overall, results show that both approaches maintain high alignment quality, even under significant bundle deformations. In the partial bundle experiment, both methods achieved good alignment results for removal of up to 50% of the original bundle. In the disrupted bundle experiment, the two methods demonstrated very high robustness to the simulated focal injury, as the FA- and tensor-based scores remained relatively constant throughout the experiment, and the FFDD dissimilarity only slightly increased. In the resampling experiment, both approaches demonstrated high tolerance to bundles' down-sampling as only a slow decline in performance was observed as the decimation factor increased.

Comparing the performance of the two approaches, we see that the pairwise alignment achieved comparable or slightly better FA- and tensor-based scores compared to the 3D alignment. This result is expected, since the pairwise approach individually aligns each pair of bundles, and therefore performs better in metrics related to pairwise alignment quality. However, the 3D alignment consistently outperforms the pairwise alignment in terms of the total FFDD dissimilarity D_N. This result supports the findings of the qualitative comparison, and empirically shows that the single-shot approach provides a globally optimal co-alignment (in terms of F_N), while the pairwise composite approach only provides an approximation. Furthermore, it seems that the 3D alignment is slightly more robust to substantial bundle deformations (e.g., in the partial bundle experiment). Based on these results we conclude that the

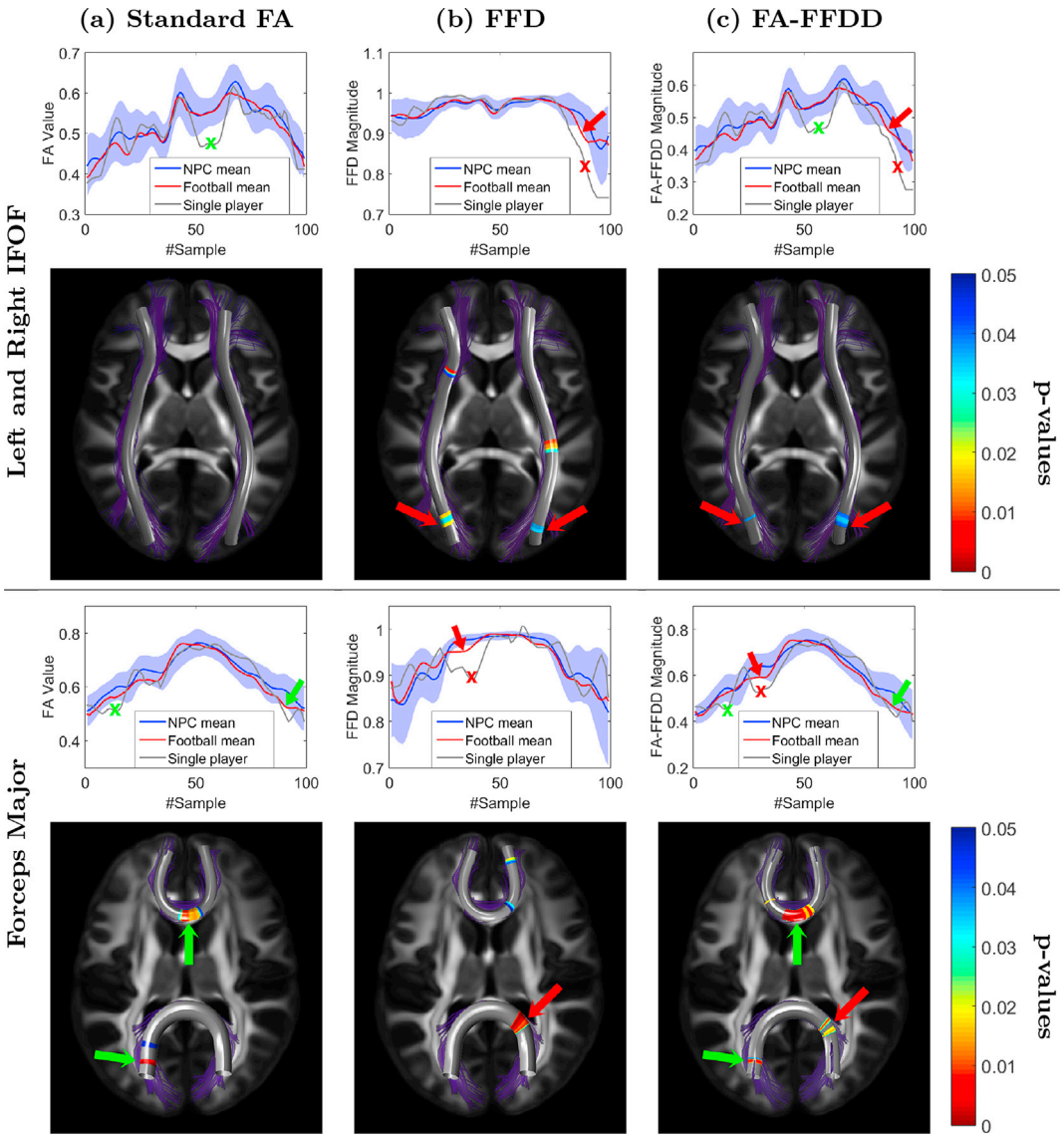

Fig. 12. Sensitivity comparison between: (a) standard FA, (b) geometry-only FFD, and (c) FA-FFDD analyses along the left and right IFOF (top panel) and Fmajor and Fminor (bottom panel) tracts. **1st and 3rd rows:** The graphs present the mean tract profile of the post-season football group (red curve) and NPC group (blue curve). The blue region represents ±1 std from the NPC group-mean profile. The tract profile of a representative football player is also presented (gray curve). All players' profiles were aligned to the corresponding standardized profiles of the NPC group. **2nd and 4th rows:** Statistically significant differences between the groups, color-coded along the tracts. The **red arrows** and '**x**'s point to areas where FA-FFDD demonstrates improved sensitivity over standard FA due to large FFD abnormality. The **green arrows** and '**x**'s point to areas where FA-FFDD demonstrates improved sensitivity over FFD analysis due to large FA abnormality.

single-shot approach is likely to be more compatible to group alignment tasks, such as multiple bundle matching and atlas creation, in which a globally optimal match is of interest.

3.4. A case study with diagnosed TBI

To test the proposed FFDD variability analysis, we first performed a pairwise comparison between two scans of a 32-year-old basketball player, diagnosed with an occipital traumatic brain injury and a frontal contusion due to contrecoup impact. Structural and diffusion MRI scans were acquired one week and 6 months after injury. Note that the hemorrhagic lesion at the frontal lobe of the player is no longer visible in the FLAIR image acquired 6 months after injury (Fig. 8a). Local differences between corresponding longitudinal FA- and MD-FFDD profiles of the Fminor (chosen due to its proximity to the lesion area) are shown in Fig. 8d. Fig. 8b–c demonstrate these differences via color-coding along the Fminor tract. Results show a significant longitudinal change at the left hemisphere part of the tract, corresponding to the lesion area, and relatively minor differences along the rest of the tract. Similar findings were demonstrated using conventional FA and MD along-tract profiles (see Fig. I1). These results should be considered as a proof of concept, demonstrating the capability of the proposed FFDD analysis to detect and localize distinct differences between fiber bundles.

3.5. Analysis of football players data

We next analyzed 13 active American-football players (mean age = 28.3, std = 6.4), compared with 17 NPCs (mean age = 26.1, std = 2.3). Detailed demographics are summarized in Table B1 (see appendix). For each subject, four FFDD tract profiles were computed (weighted by FA, MD, AD, and RD) for each of the eight examined tracts. FFDD profiles of NPCs were aligned to compute tract-specific atlases as described in section 2.4. All group-wise analyses, we used the pairwise (iterative) alignment approach described in section 2.4, as it is more

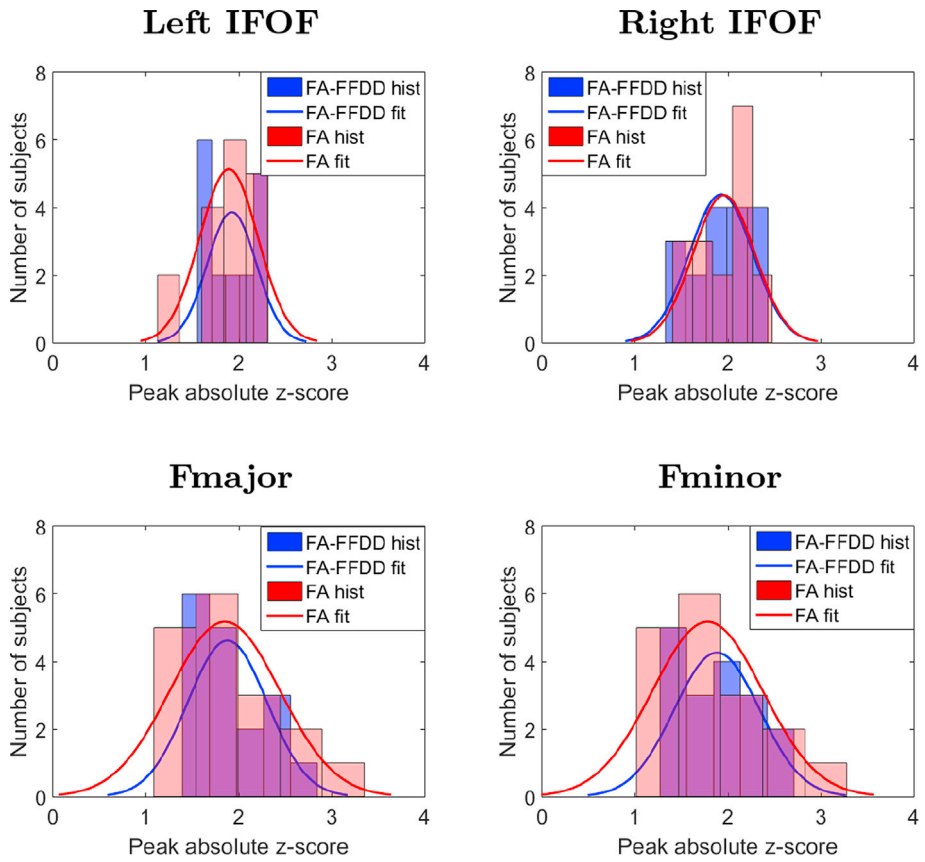

Fig. 13. Specificity analysis. Each plot presents the histogram of peak absolute z-scores of NPC subjects measured along their FA-FFDD (blue) and standard FA (red) tract profiles, with respect to their group-mean profile. A Gaussian curve was fitted to each histogram. The similar statistical spread obtained by the two measures implies that FFDD analysis did not introduce "false differences" in comparison to standard FA.

computationally efficient than the single-shot approach for aligning a large number of bundles. Examples of the resulting standardized FA-FFDD profiles are shown in Fig. 9. Notice that although the FFDD profiles may vary significantly along the tracts, their values are consistent across different subjects.

Cross-Sectional Analysis: Group-wise comparison between football players and NPCs was facilitated by first aligning all FFDD profiles of individual football players to their corresponding standardized (atlas) profiles of the NPC group, and performing statistical T-tests along the tract profiles as described in section 2.4. Fig. 10 presents a statistical analysis based on the MD-FFDD and FA-FFDD profiles of the two groups, for the left and right IFOF, Fminor and Fmajor tracts. The comparison reveals statistically significant FFDD differences (p-values < 0.05) between football players and NPCs at several locations along the tracts, mostly towards the frontal and occipital terminals of the left and right IFOF, and around the center of the Fminor and Fmajor. Note that the football group also exhibits higher std values at those locations in comparison to NPCs. This statistical spread indicates that not all football players presented abnormal FFDD values, as expected. We note that the CST and ILF tracts did not demonstrate statistically significant differences between the groups.

Longitudinal Analysis: To examine whether any temporal FFDD changes can be identified in football players throughout the playing season, we compared their mid-season and post-season scans. For this purpose, FFDD profiles of all individual players (mid- and post-season) were aligned to the standardized profile of the NPC group as described in section 2.4. Fig. 11 presents longitudinal MD-FFDD differences in the left IFOF profiles of a single player, demonstrating increased irregularities over time at the occipital part of the tract. The figure presents a similar analysis of the Fminor of another player, showing increased irregularities at the central part of the tract. Substantial longitudinal differences were also found at the *group-level*. To compare between mid- and post-season FFDD values of the entire cohort of football players, we performed paired (one-sample) pointwise T-test along their MD-FFDD profiles, and corrected the resulting p-values using FDR. Results are presented in Fig. C1 and C2 (see appendix), showing statistically significant differences at several locations within the Fminor and IFOF tracts.

3.6. Comparison to standard along-tract analysis

Sensitivity Analysis: In order to demonstrate the advantage of coupling geometry with diffusion measurements, we compared our FA-FFDD analysis with standard FA along-tract analysis, as well as to the geometry-only FFD measure, on the same football players study dataset. Similar to the FFDD analysis in section 3.3, the FA and FFD along-tract profiles of all subjects (football players and NPCs) were computed, as well as their group-mean profiles and pointwise std.

In Fig. 12a–c we present the FA, FFD, and FA-FFDD analysis results along four different bundles: the left and right IFOF, Fmajor and Fminor tracts. The sensitivity of each of the three measures is compared for both group-wise and individual subject analysis. For the group-wise level, we performed pointwise unpaired (two-sample) T-tests along the subjects' FA, FFD and FA-FFDD profiles of the two groups. As shown in Fig. 12, the resulting (FDR corrected) p-values demonstrate statistically significant FA-FFDD differences near the occipital part of the IFOF and the center of the Fmajor tract (marked by red arrows), that were missed by the standard FA analysis. Note that in this case, the enhanced sensitivity of the FA-FFDD measure was made possible by the additional geometrical information incorporated into our descriptor, as shown in Fig. 12b. For the Fminor tract, the FA-FFDD analysis demonstrated statistically significant

differences around the center of the Fminor tract (marked by green arrows), that were missed by the geometry-only FFD analysis. Here, the diffusion information was the contributing factor to the FA-FFDD's improved sensitivity, as shown in Fig. 12a. The restraining effect of the coupled FFDD descriptor is also demonstrated in this comparison. In locations where either standard FA or FFD indicated statistically significant differences, but the disagreement between them was large enough, they were not translated into statistically significant FA-FFDD differences (for example, the FFD differences found at the center of the IFOF).

To demonstrate the improved sensitivity at the single-subject level as well, the FA, FFD, and FA-FFDD tract profiles of individual football players were compared to the NPC group atlas (see Fig. D1 in Appendix D). We demonstrate this comparison for a representative football player in Fig. 12 (see gray curves in the 1st and 3rd rows of the figure). In locations marked by red 'x', enhanced FA-FFDD sensitivity was demonstrated in comparison to standard FA, due to large FFD abnormalities. Similarly, in locations marked by green 'x', improved FA-FFDD sensitivity was demonstrated in comparison to the geometry-only FFD analysis due to large FA abnormalities.

Specificity Analysis: We next examine the specificity of the FFDD measure with respect to standard FA. In the absence of a ground-truth dataset, this was performed using the scans of NPC subjects, demonstrating that the proposed FFDD measure does not introduce large differences when they are not expected. For this purpose, we used the FA-FFDD and standard FA tract profiles of all 17 NPC subjects. For each subject, we calculated the maximal (peak) value of the absolute z-score along its FA-FFDD and FA tract profiles. This was done in a leave-one-out fashion, such that the z-score was measured with respect to the remaining 16 subjects of the NPC group. In Fig. 13 we present a histogram of these measurements for the same bundles analyzed in the sensitivity analysis (left and right IFOF, Fmajor and Fminor). Results show that a similar average peak z-score is obtained when using FA-FFDD and standard FA, while the variance is lower in the FA-FFDD case. This suggests that the proposed FFDD measure does not impair specificity, and does not introduce "false-differences" with respect to standard FA analysis.

4. Discussion

We presented a comprehensive framework for WM tract-specific analysis, addressing fiber bundle modeling, alignment and variability analysis. We introduced the novel concept of *Fiber-Flux Diffusion Density* (FFDD) profiles for quantitative analysis of fiber bundles, reflecting local and subtle WM structural variations. We demonstrated how spatial normalization of bundles can be achieved by aligning their FFDD profiles, thus facilitating pair-wise comparisons as well as group-wise statistical analysis. We tested our method on two clinical datasets of contact-sports players, showing promising results in WM abnormalities detection and localization.

The key idea of the proposed FFDD model is the coupling of WM diffusion properties with fiber bundle geometry. By doing so, a multi-scale description of WM tracts is obtained, as both microscopic (i.e., diffusion indices) and macroscopic (i.e., bundles geometry) structural features are utilized. As shown in our sensitivity analysis, this combination is more sensitive to detecting WM abnormalities with respect to standard diffusion parameters alone (see Fig. 12). While the advantages of the combined measure are clearly demonstrated in our experiments, the clinical interpretability of the results may not be straight forward. We note, however, that the coupled FFDD descriptor can always be displayed alongside the standard FA and the geometric FFD measure, for a disentangled interpretation of the results.

Our fiber bundle alignment method is another key component in the proposed FFDD framework, which unlike many WM analysis techniques, does not require an external registration tool. The alignment is founded on a unique FFDD-based dissimilarity measure between bundles, which naturally emerges from our model. Representing bundles by their mean trajectory, we addressed their alignment as a curve-matching problem. Specifically, we used the FMM to find the optimal matching of FFDD profiles with sub-sampling resolution. We showed that using FMM allows symmetrical pairwise bundle alignment, as well as single-shot co-alignment of multiple bundles. Moreover, comparing the performance of the well-known DTI-TK registration with the proposed alignment method, for both FA and tensor-based matching criteria (see Table 1 and Fig. 4), highlights the advantages of the latter, in particular its robustness to areas with high inter-subject variability such as the terminals of the IFOF (see Fig. 5 for example). We believe that a key contributor to these results is the coupling of diffusion and geometry information by the FFDD descriptor. Since fiber bundles are not uniform, as their central parts tend to be more geometrically coherent than their edges, FFDD differences between them along the coherent part of their trajectories are mainly due to diffusion values. However, towards the edges where bundles are more spread out, it is both geometry and diffusion that account for these differences. Since the proposed alignment method is designed to minimize FFDD dissimilarities, it takes into consideration both diffusion and geometrical differences along the entire bundle trajectory, without preferring one measure over another. This is demonstrated in Fig. 5, showing a consistent alignment quality along the bundle trajectory when using FFDD, for both FA and tensor-based matching criteria. The strength of the proposed alignment method was further demonstrated in handling different types of bundle deformations. As shown in Fig. 7, our method was able to maintain high alignment quality even in the presence of missing bundle segments, simulated focal injuries, and bundle down-sampling. Lastly, we believe that one of the main advantages of the proposed alignment framework is its applicability to the construction of tract-specific FFDD atlases, by efficiently computing a group template from a cohort of tract profiles (see Fig. 9). Thus, cross-sectional and longitudinal studies, for the purpose of variability analysis and anomaly detection, can be facilitated without using an external registration tool.

We evaluated the entire FFDD framework (i.e., both modeling and alignment) on two diffusion MRI datasets of contact-sports players: a basketball player with a confirmed frontal hemorrhagic contusion, which was used as a case-study, and a cohort of active American-football players who are likely to be exposed to repetitive head trauma. FFDD analysis of the basketball player revealed substantial longitudinal differences at the forceps minor tract, localized near the hemorrhagic lesion. We consider this result to be a "proof of concept", demonstrating our method's ability to reliably reflect and localize notable WM damage. Group-wise analysis of the football players' dataset, on the other hand, is much more challenging since all examined players are young, otherwise-healthy athletes with no definitive clinical diagnosis. Nevertheless, our hypothesis was that WM abnormalities were likely to be found in some players due to repetitive head traumas. Accommodating these uncertainties due to the heterogeneity of the football players group, our method was sufficiently sensitive to detect mild WM abnormalities, which in some cases were not reflected by either diffusion-based or geometry-based analysis alone. The FFDD abnormalities were identified at specific tract locations, mostly near the frontal and occipital terminals of the left and right IFOF, and medial parts of the Fminor and Fmajor tracts. These areas also demonstrated statistically significant FFDD differences (p-value<0.05) between football players and NPCs. In the absence of a ground-truth (that can be only available *ex-vivo*), we support these findings by noting that the anomalies were only found in certain fiber tracts and at specific locations across different players, i.e., around the central parts of the Fminor and Fmajor and towards the terminals of the IFOF. Moreover, the results are in line with previous findings of mTBI studies (Hulkower et al., 2013) as well as with finite-element computational models of mTBI (Bigler, 2018), both suggesting these specific tracts as particularly vulnerable to head trauma. Furthermore, in agreement with our findings (Bahrami et al., 2016), reports localized abnormalities at the IFOF terminals in young football players, pointing out these specific regions as susceptible to mTBIs, due to the forces acting on the interface between WM and gray matter during impact.

In addition to cross-sectional analysis, our framework also supports

longitudinal comparisons. Our experiments revealed substantial temporal aggravation of FFDD abnormalities at spatially-consistent locations across several football players, by comparing their mid-season and post-season scans (see Fig. 11 and Appendix C). These findings are consistent with studies that examined the cumulative effect of repetitive head trauma on the WM structural integrity of contact-sports players (Bahrami et al., 2016; Bazarian et al., 2014).

4.1. Possible applications

In this work we have demonstrated the proposed FFDD method for detection and localization of mTBI-induced WM abnormalities. However, we note that our framework is general, and can be used for the assessment of other neurological conditions in which structural WM damage is likely to be found. Moreover, the flexibility of our framework supports the use of any scalar measurement of choice (e.g., generalized FA), and is not limited to DTI-derived diffusion parameters. We further note that the method can be used exclusively for the task of fiber bundle alignment, thus facilitating any subsequent quantitative analysis.

4.2. Limitations and future directions

The proposed framework is designed for along-tract analysis. As such, it is more applicable to fiber bundles that are relatively long compared to their cross-section diameter. This includes some major fiber bundles such as the IFOF and CST, as well as U-shaped tracts such as the parcelled parts of the corpus callosum. However, fiber bundles with multiple branches (e.g., the superior longitudinal fasciculus) or with a more complex topology (e.g., the cingulum tract) may require some adjustments prior to analysis with our method, for example clipping the tracts' edges or parcellation into sub-segments.

Whenever a 3D bundle is analyzed using a 1D model, as in along-tract analysis, some of the original information regarding the bundle is bound to be lost due to projection of volumetric data to a lower-dimensional representation. To alleviate this issue, an adequate within-bundle point correspondence is required such that sets of projected (or averaged) measurements would have low variance. In this work, this was addressed to some extent by *not restricting* the bundle's cross-sections, along which measurements are taken, to be perpendicular to the mean streamline of the bundle. Instead, the cutting plane was oriented such that the geometrical fiber-flux density (FFD) through it is maximized (as detailed in Appendix A). This allows for a decent structural correspondence across individual streamlines to be obtained, even in areas of high curvature and streamline spreads (see Appendix G for quantitative evaluation of within-bundle correspondence quality). We note, however, that a more flexible correspondence may be achieved by allowing corresponding points to stray off a planar cross-section (e.g., as suggested by (O'Donnell et al., 2009)).

We also note that due to the limited angular resolution of the clinical DWI scans used in this work (33 gradient directions), all experiments were based on DTI data (and DTI-derived indices), followed by deterministic tractography. The limitations of these tensor-based methodologies, and their inability to faithfully model multiple crossing fibers within a single voxel in particular, were discussed by the diffusion MRI community (Descoteaux and Poupon, 2012; Jones, 2010; O'Donnell and Pasternak, 2015). Nevertheless, we note that the proposed framework only requires the fiber bundle tractogram and a corresponding scalar measurements field. Therefore, it is also suitable for the analysis of High Angular Resolution Diffusion Imaging (HARDI) data. In fact, since HARDI data provides an improved estimation of fibers' orientation and fiber crossings' modeling, it is likely to enhance the detection of subtle structural WM variations using our method. In addition to HARDI data, using probabilistic tractography algorithms rather than deterministic tracking may better capture the full complexity of fiber tracts' structure, thus potentially refining the quality of the FFDD analysis.

Acknowledgment

This study was partially supported by The Israel Science Foundation (1638/16); The Israel Defense Forces (IDF) Medical Corps and Directorate of Defense Research & Development, Israel Ministry of Defense (IMOD DDR&D).

Appendix A. Supplementary data

Supplementary data to this article can be found online at https://doi.org/10.1016/j.neuroimage.2019.05.003.

References

Andersson, J.L., Jenkinson, M., Smith, S., et al., 2007. Non-linear Registration, Aka Spatial Normalisation Fmrib Technical Report Tr07ja2, vol. 2. *FMRIB Analysis Group of the University of Oxford*, pp. 1–21.

Bahrami, N., Sharma, D., Rosenthal, S., Davenport, E.M., Urban, J.E., Wagner, B., Jung, Y., Vaughan, C.G., Gioia, G.A., Stitzel, J.D., et al., 2016. Subconcussive head impact exposure and white matter tract changes over a single season of youth football. Radiology 281, 919–926.

Basser, P.J., Pierpaoli, C., 2011. Microstructural and physiological features of tissues elucidated by quantitative-diffusion-tensor MRI. J. Magn. Reson. 213 (2), 560–570.

Baugh, C.M., Stamm, J.M., Riley, D.O., Gavett, B.E., Shenton, M.E., Lin, A., Nowinski, C.J., Cantu, R.C., McKee, A.C., Stern, R.A., 2012. Chronic traumatic encephalopathy: neurodegeneration following repetitive concussive and subconcussive brain trauma. Brain imaging and behavior 6 (2), 244–254.

Bazarian, J.J., Zhu, T., Zhong, J., Janigro, D., Rozen, E., Roberts, A., Javien, H., Merchant-Borna, K., Abar, B., Blackman, E.G., 2014. Persistent, long-term cerebral white matter changes after sports-related repetitive head impacts. PLoS One 9 (4) p. e94734.

Benjamini, Y., Hochberg, Y., 1995. Controlling the false discovery rate: a practical and powerful approach to multiple testing. J. R. Stat. Soc. Ser. B 289–300.

Benou, I., Veksler, R., Friedman, A., Raviv, T.R., 2018. Fiber-flux diffusion density for white matter tracts analysis: application to mild anomalies localization in contact sports players. In: Computational Diffusion MRI, pp. 191–204.

Bigler, E.D., 2018. Structural neuroimaging in sport-related concussion. Int. J. Psychophysiol. 132, 105–123.

Borja, M.J., Chung, S., Lui, Y.W., 2018. Diffusion MR imaging in mild traumatic brain injury. Neuroimaging Clinics 28 (1), 117–126.

Bouix, S., Pasternak, O., Rathi, Y., Pelavin, P.E., Zafonte, R., Shenton, M.E., 2013. Increased gray matter diffusion anisotropy in patients with persistent post-concussive symptoms following mild traumatic brain injury. PLoS One 8 (6) p. e66205.

Chung, M.K., Adluru, N., Lee, J.E., Lazar, M., Lainhart, J.E., Alexander, A.L., 2010. Cosine series representation of 3D curves and its application to white matter fiber bundles in diffusion tensor imaging. Stat. Interface 3 (1), 69.

Cohen, I., Ayache, N., Sulger, P., 1992. Tracking points on deformable objects using curvature information. In: European Conference on Computer Vision, pp. 458–466.

Colby, J.B., Soderberg, L., Lebel, C., Dinov, I.D., Thompson, P.M., Sowell, E.R., 2012. Along-tract statistics allow for enhanced tractography analysis. Neuroimage 59 (4), 3227–3242.

Corouge, I., Gouttard, S., Gerig, G., 2004. "Towards a shape model of white matter fiber bundles using diffusion tensor MRI," in *Biomedical Imaging: Nano to Macro*. In: 2004. IEEE International Symposium on, pp. 344–347.

Corouge, I., Fletcher, P.T., Joshi, S., Gouttard, S., Gerig, G., 2006. Fiber tract-oriented statistics for quantitative diffusion tensor MRI analysis. Med. Image Anal. 10 (5), 786–798.

de Groot, M., Vernooij, M.W., Klein, S., Ikram, M.A., Vos, F.M., Smith, S.M., Niessen, W.J., Andersson, J.L., 2013. Improving alignment in tract-based spatial statistics: evaluation and optimization of image registration. Neuroimage 76, 400–411.

Descoteaux, M., Poupon, C., 2012. Diffusion-weighted MRI. Comprehensive Biomedical Physics 3 (6), 81–97.

Fan, Q., Witzel, T., Nummenmaa, A., Van Dijk, K.R., Van Horn, J.D., Drews, M.K., Somerville, L.H., Sheridan, M.A., Santillana, R.M., Snyder, J., et al., 2016. MGH–USC human connectome project datasets with ultra-high b-value diffusion MRI. Neuroimage 124, 1108–1114.

Frenkel, M., Basri, R., 2003. Curve matching using the fast marching method. In: International Workshop on Energy Minimization Methods in Computer Vision and Pattern Recognition, pp. 35–51.

Garyfallidis, E., Brett, M., Correia, M.M., Williams, G.B., Nimmo-Smith, I., 2012. Quickbundles, a method for tractography simplification. Front. Neurosci. 6, 175.

Garyfallidis, E., Ocegueda, O., Wassermann, D., Descoteaux, M., 2015. Robust and efficient linear registration of white-matter fascicles in the space of streamlines. Neuroimage 117, 124–140.

Glozman, T., Bruckert, L., Pestilli, F., Yecies, D.W., Guibas, L.J., Yeom, K.W., 2018. Framework for shape analysis of white matter fiber bundles. Neuroimage 167, 466–477.

Gorodissky, O., Sharon, A., Danov, A., Friedman, A., Raviv, T.R., 2018. Symmetry-based analysis of diffusion MRI for the detection of brain impairments. In: 2018 25th IEEE International Conference on Image Processing (ICIP). IEEE, pp. 376–379.

Håberg, A., Olsen, A., Moen, K., Schirmer-Mikalsen, K., Visser, E., Finnanger, T., Evensen, K., Skandsen, T., Vik, A., Eikenes, L., 2015. White matter microstructure in chronic moderate-to-severe traumatic brain injury: impact of acute-phase injury-

related variables and associations with outcome measures. J. Neurosci. Res. 93 (7), 1109–1126.
Heimer, L., 2012. The Human Brain and Spinal Cord: Functional Neuroanatomy and Dissection Guide. Springer Science & Business Media.
Hulkower, M., Poliak, D., Rosenbaum, S., Zimmerman, M., Lipton, M.L., 2013. A decade of DTI in traumatic brain injury: 10 years and 100 articles later. Am. J. Neuroradiol. 34 (11), 2064–2074.
Jiang, H., Van Zijl, P.C., Kim, J., Pearlson, G.D., Mori, S., Dtistudio, ", 2006. Resource program for diffusion tensor computation and fiber bundle tracking. Comput. Methods Progr. Biomed. 81 (2), 106–116.
Jones, D.K., 2010. Challenges and limitations of quantifying brain connectivity in vivo with diffusion MRI. Imaging Med. 2 (3), 341.
Khatami, M., Schmidt-Wilcke, T., Sundgren, P.C., Abbasloo, A., Schölkopf, B., Schultz, T., BundleMAP, ", 2017. Anatomically localized classification, regression, and hypothesis testing in diffusion MRI. Pattern Recogn. 63, 593–600.
Klein, J., Hermann, S., Konrad, O., Hahn, H.K., Peitgen, H.-O., 2007. Automatic quantification of DTI parameters along fiber bundles. In: Bildverarbeitung für die Medizin 2007, pp. 272–276.
Mårtensson, J., Nilsson, M., Ståhlberg, F., Sundgren, P.C., Nilsson, C., van Westen, D., Larsson, E.-M., Lätt, J., 2013. Spatial analysis of diffusion tensor tractography statistics along the inferior fronto-occipital fasciculus with application in progressive supranuclear palsy. Magnetic Resonance Materials in Physics, Biology and Medicine 26 (6), 527–537.
Mori, S., Oishi, K., Jiang, H., Jiang, L., Li, X., Akhter, K., Hua, K., Faria, A.V., Mahmood, A., Woods, R., et al., 2008. Stereotaxic white matter atlas based on diffusion tensor imaging in an ICBM template. Neuroimage 40 (2), 570–582.
Olivetti, E., Sharmin, N., Avesani, P., 2016. Alignment of tractograms as graph matching. Front. Neurosci. 10, 554.
O'Donnell, L.J., Pasternak, O., 2015. Does diffusion MRI tell us anything about the white matter? an overview of methods and pitfalls. Schizophr. Res. 161 (1), 133–141.
O'Donnell, L.J., Westin, C.-F., Golby, A.J., 2009. Tract-based morphometry for white matter group analysis. Neuroimage 45 (3), 832–844.
O'Donnell, L.J., Wells, W.M., Golby, A.J., Westin, C.-F., 2012. Unbiased groupwise registration of white matter tractography. In: International Conference on Medical Image Computing and Computer-Assisted Intervention, pp. 123–130.
Prasad, G., Joshi, S.H., Jahanshad, N., Villalon-Reina, J., Aganj, I., Lenglet, C., Sapiro, G., McMahon, K.L., de Zubicaray, G.I., Martin, N.G., et al., 2014. Automatic clustering and population analysis of white matter tracts using maximum density paths. Neuroimage 97, 284–295.
Raffelt, D.A., Tournier, J.-D., Smith, R.E., Vaughan, D.N., Jackson, G., Ridgway, G.R., Connelly, A., 2017. Investigating white matter fibre density and morphology using fixel-based analysis. Neuroimage 144, 58–73.
Sebastian, T.B., Klein, P.N., Kimia, B.B., 2003. On aligning curves. IEEE Trans. Pattern Anal. Mach. Intell. 25 (1), 116–125.
Sethian, J.A., 1996. A fast marching level set method for monotonically advancing fronts. Proc. Natl. Acad. Sci. Unit. States Am. 93 (4), 1591–1595.
Sharp, D.J., Scott, G., Leech, R., 2014. Network dysfunction after traumatic brain injury. Nat. Rev. Neurol. 10 (3), 156.
Shenton, M.E., Hamoda, H., Schneiderman, J., Bouix, S., Pasternak, O., Rathi, Y., Vu, M.-A., Purohit, M.P., Helmer, K., Koerte, I., et al., 2012. A review of magnetic resonance imaging and diffusion tensor imaging findings in mild traumatic brain injury. Brain imaging and behavior 6 (2), 137–192.
Smith, S.M., Jenkinson, M., Johansen-Berg, H., Rueckert, D., Nichols, T.E., Mackay, C.E., Watkins, K.E., Ciccarelli, O., Cader, M.Z., Matthews, P.M., et al., 2006. Tract-based spatial statistics: voxelwise analysis of multi-subject diffusion data. Neuroimage 31 (4), 1487–1505.
Tagliasacchi, A., Zhang, H., Cohen-Or, D., 2009. Curve skeleton extraction from incomplete point cloud. ACM Trans. Graph. 28, 71.
Wang, Y., Gupta, A., Liu, Z., Zhang, H., Escolar, M.L., Gilmore, J.H., Gouttard, S., Fillard, P., Maltbie, E., Gerig, G., et al., 2011. DTI registration in atlas based fiber analysis of infantile krabbe disease. Neuroimage 55 (4), 1577–1586.
Wang, D., Luo, Y., Mok, V.C., Chu, W.C., Shi, L., 2016. Tractography atlas-based spatial statistics: statistical analysis of diffusion tensor image along fiber pathways. Neuroimage 125, 301–310.
Wang, Y., Shen, Y., Liu, D., Li, G., Guo, Z., Fan, Y., Niu, Y., 2017. Evaluations of diffusion tensor image registration based on fiber tractography. Biomed. Eng. Online 16 (1), 9.
Yap, P.-T., Wu, G., Zhu, H., Lin, W., Shen, D., 2009. TIMER: tensor image morphing for elastic registration. Neuroimage 47 (2), 549–563.
Yeatman, J.D., Dougherty, R.F., Myall, N.J., Wandell, B.A., Feldman, H.M., 2012. Tract profiles of white matter properties: automating fiber-tract quantification. PLoS One 7 (11) p. e49790.
Yeh, F.-C., Verstynen, T.D., Wang, Y., Fernández-Miranda, J.C., Tseng, W.-Y.I., 2013. Deterministic diffusion fiber tracking improved by quantitative anisotropy. PLoS One 8 (11) p. e80713.
Yendiki, A., Panneck, P., Srinivasan, P., Stevens, A., Zöllei, L., Augustinack, J., Wang, R., Salat, D., Ehrlich, S., Behrens, T., et al., 2011. Automated probabilistic reconstruction of white-matter pathways in health and disease using an atlas of the underlying anatomy. Front. Neuroinf. 5, 23.
Yeo, B.T., Vercauteren, T., Fillard, P., Peyrat, J.-M., Pennec, X., Golland, P., Ayache, N., Clatz, O., 2009. DT-REFinD: diffusion tensor registration with exact finite-strain differential. IEEE Trans. Med. Imaging 28 (12), 1914–1928.
Younes, L., 1998. Computable elastic distances between shapes. SIAM J. Appl. Math. 58 (2), 565–586.
Yushkevich, P.A., Zhang, H., Simon, T.J., Gee, J.C., 2008. Structure-specific statistical mapping of white matter tracts. Neuroimage 41 (2), 448–461.
Zhang, H., Yushkevich, P.A., Alexander, D.C., Gee, J.C., 2006. Deformable registration of diffusion tensor MR images with explicit orientation optimization. Med. Image Anal. 10 (5), 764–785.
Zhang, H., Awate, S.P., Das, S.R., Woo, J.H., Melhem, E.R., Gee, J.C., Yushkevich, P.A., 2010. A tract-specific framework for white matter morphometry combining macroscopic and microscopic tract features. Med. Image Anal. 14 (5), 666–673.
Zhang, Z., Descoteaux, M., Zhang, J., Girard, G., Chamberland, M., Dunson, D., Srivastava, A., Zhu, H., 2018. Mapping population-based structural connectomes. Neuroimage 172, 130–145.
Zvitia, O., Mayer, A., Shadmi, R., Miron, S., Greenspan, H.K., 2010. Co-registration of white matter tractographies by adaptive-mean-shift and Gaussian mixture modeling. IEEE Trans. Med. Imaging 29 (1), 132–145.